

# First-principles calculations of $\beta''$ -Mg<sub>5</sub>Si<sub>6</sub>/ $\alpha$ -Al interfaces

Y. Wang<sup>a,\*</sup>, Z.-K. Liu<sup>a</sup>, L.-Q. Chen<sup>a</sup>, C. Wolverton<sup>b,1</sup>

<sup>a</sup> *Materials Science and Engineering, The Pennsylvania State University, State College, PA 16802-5006, USA*

<sup>b</sup> *Ford Research and Advanced Engineering, MD3083/SRL, Dearborn, MI 48121-2053, USA*

Received 26 January 2007; received in revised form 11 June 2007; accepted 29 June 2007

Available online 29 August 2007

## Abstract

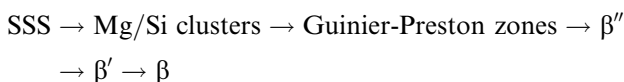
The metastable  $\beta''$ -Mg<sub>5</sub>Si<sub>6</sub> phase is often the most effective hardening precipitate in Al-rich Al–Mg–Si alloys. Two important factors that control the precipitate morphology are the strain energy and the interfacial energy between the precipitate and the matrix. By means of a first-principles supercell approach and density functional theory calculations, we have studied the interfacial properties between  $\beta''$ -Mg<sub>5</sub>Si<sub>6</sub> and  $\alpha$ -Al. We carefully construct a large number of interfacial cells in order to elucidate preferred interfacial terminations and orientations, as well as atom alignment and intermixing across the interface. Each of the low-energy interfaces we found possesses two key attributes: a high number of Al–Si bonds across the interface, and a face-centered cubic topological alignment of atoms across those interfaces. Our first-principles results yield quantitative values for the interfacial energies, lattice mismatches and strain energies that can be used in future predictions of precipitate morphologies as a function of size.

© 2007 Acta Materialia Inc. Published by Elsevier Ltd. All rights reserved.

**Keywords:**  $\beta''$ -Mg<sub>5</sub>Si<sub>6</sub>/ $\alpha$ -Al interface; Interfacial energy; Lattice mismatch; First-principles

## 1. Introduction

Precipitation hardening is utilized to strengthen a wide variety of alloy systems. An example is the class of commercially important Al–Mg–Si based alloys which are strengthened by a number of metastable precipitate phases [1–12], where the needle-shaped  $\beta''$ -Mg<sub>5</sub>Si<sub>6</sub> precipitates are often the main contributor to hardening [11]. Beginning with the supersaturated solid solution (SSS), the generic precipitation sequence in Al–Mg–Si alloys is generally believed to be [12]:



In practice, the sequence can be even more complex [1,3,10–14], and a number of other metastable phases, such

as U<sub>2</sub>, U<sub>1</sub> and B', may also form along with  $\beta'$ , depending on alloy composition and the heat treatment time and temperature.

One of the key factors that control the mechanical properties of precipitate-hardened alloys is the precipitate morphology, i.e. the size and shape of precipitates. In order to predict [15,16] the precipitate microstructural evolution and thus mechanical properties, it is critical that the thermodynamic driving forces and kinetic mechanisms that lead to various precipitate shapes be understood.

The morphology of a precipitate is primarily determined by two competing energetic contributions, i.e. the interfacial energy between the precipitate and the matrix and the coherency elastic strain energy generated due to the lattice mismatch between the precipitate and the matrix. Obtaining these quantities directly from experiments can be difficult due to the metastable nature of many precipitates. For example, in many cases, including  $\beta''$ -Mg<sub>5</sub>Si<sub>6</sub>, only the constrained lattice parameters are available experimentally (e.g. from high-resolution transmission electron microscopy (TEM) or diffraction

\* Corresponding author. Tel.: +1 814 8650389; fax: +1 814 8652917.

E-mail address: [yuw3@psu.edu](mailto:yuw3@psu.edu) (Y. Wang).

<sup>1</sup> Present address: Department of Materials Science and Engineering, Northwestern University, 2220 Campus Drive, Evanston, IL 60208, USA.

approaches [11,17]). But experimental data for stress-free lattice parameters (and hence the lattice mismatch), as well as elastic constants and interfacial energies, are not typically available. First-principles total energy and crystal structure calculations provide a computational tool capable of giving quantitative predictions for these hard-to-measure quantities.

The main objective of this paper is to search for low energy interfaces between the  $\beta''$ - $\text{Mg}_5\text{Si}_6$  precipitate and the  $\alpha$ -Al matrix from a first-principles approach. Extensive calculations were performed to examine the effects of interfacial termination, atomic alignment and intermixing [11], and interfacial orientations [18,19]. Though interfacial energies have been previously calculated using first-principles calculations in other systems (see e.g. [20–23]), almost all of these previous calculations have been focused on systems where both phases are high-symmetry cubic phases, often with simple small-unit-cell crystal structures. In contrast, the precipitate/matrix interfaces studied in this work involve the relatively low-symmetry monoclinic  $\beta''$ - $\text{Mg}_5\text{Si}_6$  precipitate with a complex stoichiometry and crystal structure, and a high symmetry cubic  $\alpha$ -Al matrix. As a result of the complexity of this system, there are a large number of degrees of freedom to consider in constructing the interfaces, including where to “cut” the crystals of the matrix and precipitate and how to “join” them – interfacial orientation, interfacial termination, atom alignment and atomic arrangement near the interface. In the following sections, the crystal structure of  $\beta''$ - $\text{Mg}_5\text{Si}_6$ , its relationship with  $\alpha$ -Al (face-centered cubic, fcc) and the supercell models for the  $\beta''$ - $\text{Mg}_5\text{Si}_6/\alpha$ -Al interface are described. We then give first-principles results for the interfacial energies and strain energies, as well as the stress-free mismatch in  $\beta''$ - $\text{Mg}_5\text{Si}_6/\alpha$ -Al. In addition, we investigate a recently proposed model for one of the  $\beta''$ - $\text{Mg}_5\text{Si}_6/\alpha$ -Al interfaces in which an intermixing tendency across this interface has been deduced from high-resolution electron microscopy (HREM) and electron diffraction (ED) measurements [11].

## 2. Crystal structures and interface models

### 2.1. Structural relationship between $\beta''$ - $\text{Mg}_5\text{Si}_6$ and $\alpha$ -Al

Fig. 1 illustrates the structural similarity [11] between  $\beta''$ - $\text{Mg}_5\text{Si}_6$  and fcc  $\alpha$ -Al by showing a 22-atom supercell of the  $\alpha$ -Al fcc lattice in the form of a conventional monoclinic unit cell (CMUC) of  $\beta''$ - $\text{Mg}_5\text{Si}_6$ . In this representation, the lattice vector  $\mathbf{b}_{\beta''}$  ( $[010]$ ) of the  $\beta''$ - $\text{Mg}_5\text{Si}_6$  is parallel to the  $[001]$  axis of  $\alpha$ -Al ( $\mathbf{b}_{\beta''} = \mathbf{c}_{\text{Al}}$ ) and the other two lattice vectors of  $\beta''$ - $\text{Mg}_5\text{Si}_6$  are defined by  $\mathbf{a}_{\beta''} = 2\mathbf{a}_{\text{Al}} + 3\mathbf{b}_{\text{Al}}$  (i.e. the  $[230]$  direction in  $\alpha$ -Al) and  $\mathbf{c}_{\beta''} = -1.5\mathbf{a}_{\text{Al}} + 0.5\mathbf{b}_{\text{Al}}$  (i.e. the  $[\bar{3}10]$  direction of  $\alpha$ -Al). As noted in Ref. [11], even a precise one-to-one atom mapping between  $\beta''$ - $\text{Mg}_5\text{Si}_6$  and  $\alpha$ -Al can be obtained if one shifts the corner Mg and  $\mathbf{a}_{\beta''}/2$  Mg atoms by  $\mathbf{b}_{\beta''}/2$ .

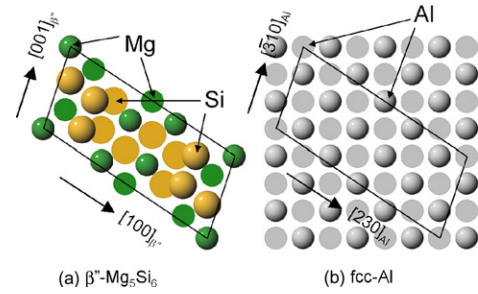


Fig. 1. The crystal structure of  $\beta''$ - $\text{Mg}_5\text{Si}_6$  (a) and its relation with  $\alpha$ -Al (b). Mg: green (small balls); Si: orange (large balls); Al: gray. The solid balls show atoms at the paper surface and flat plates show atoms at  $\mathbf{b}_{\beta''}/2$  ( $\sim 0.2025$  nm) into the paper surface. It can be seen that the one-to-one atom correspondence can be assigned between the two parallelograms, with only the Mg atom at the corner of the  $\beta''$ - $\text{Mg}_5\text{Si}_6$  parallelogram being shifted  $\mathbf{b}_{\beta''}/2$  if being compared the  $\alpha$ -Al parallelogram. Note that the Mg atom located at the  $[100]_{\beta''}$  side of the  $\beta''$ - $\text{Mg}_5\text{Si}_6$  parallelogram is equivalent to corner Mg atom by translational symmetry. (For interpretation of the references to colour in this figure legend, the reader is referred to the web version of this article.)

### 2.2. Interfacial orientations

A reconstructed exit wave of a typical  $\beta''$ - $\text{Mg}_5\text{Si}_6$  needle in  $\alpha$ -Al by Andersen et al. [11] showed the existence of two types of interfaces parallel to the needle axis  $\mathbf{b}_{\beta''}$  (needle- $\parallel$ ), i.e. one parallel to the  $(100)$  crystal plane of  $\beta''$ - $\text{Mg}_5\text{Si}_6$  and another parallel to the  $(001)$  crystal plane of  $\beta''$ - $\text{Mg}_5\text{Si}_6$ . Along with these two observed interfacial orientations, for completeness, we assume a third interface be the plane paralleling to the  $(010)$  crystal plane of  $\beta''$ - $\text{Mg}_5\text{Si}_6$  (needle- $\perp$ ). The interfacial orientation relations for these three types of interfaces are summarized as follows:

- A:  $(130)_{\text{Al}} \parallel (100)_{\beta''}$  (needle- $\parallel$ )
- B:  $(001)_{\text{Al}} \parallel (010)_{\beta''}$  (needle- $\perp$ )
- C:  $(\bar{3}20)_{\text{Al}} \parallel (001)_{\beta''}$  (needle- $\parallel$ )

where the labels A, B and C are used simply to reflect, respectively, the interfacial orientation direction of  $\beta''$ - $\text{Mg}_5\text{Si}_6$  for that interface.

## 3. Supercells

In our first-principles calculations, we adopt coherent models along all interfacial orientations considered. Table 1 summarizes the interfacial orientations, alignments, terminations and interfacial intermixing of all interfacial supercells considered in this paper.

The conventional monoclinic unit cell (CMUC) shown in Fig. 1 is used as the “building block”: the interfacial supercells are built using multiple CMUC units, with the 22 atoms of each CMUC having stoichiometries  $\text{Al}_{22}$  or  $\text{Mg}_{10}\text{Si}_{12}$  on either side of the interface. It should be noted that if one shifts the corner Mg atom of  $\beta''$ - $\text{Mg}_5\text{Si}_6$  (equivalent to the  $\mathbf{a}_{\beta''}/2$  Mg atom) by  $\mathbf{b}_{\beta''}/2$ , the

Table 1  
Description of interfacial cells constructed<sup>a</sup>

Supercell	Orientation	Alignment	# Atoms	Shift interface	Equivalent interfaces	# Al–Mg bonds	# Al–Si bonds
X <sub>1</sub>	(130) <sub>Al</sub>    (100) <sub>β''</sub>	β''	44	N	N	14	6
X <sub>2</sub>	(130) <sub>Al</sub>    (100) <sub>β''</sub>	β''	44	Y	N	16	20
X <sub>3</sub>	(130) <sub>Al</sub>    (100) <sub>β''</sub>	β''	44	Y	N	12	13
X <sub>4</sub>	(130) <sub>Al</sub>    (100) <sub>β''</sub>	β''	44	Y	N	6	14
X <sub>5</sub>	(130) <sub>Al</sub>    (100) <sub>β''</sub>	Pre-β''	44	N	N	11	9
X <sub>6</sub>	(130) <sub>Al</sub>    (100) <sub>β''</sub>	Pre-β''	44	Y	N	23	22
X <sub>7</sub>	(130) <sub>Al</sub>    (100) <sub>β''</sub>	Pre-β''	44	Y	N	16	16
X <sub>8</sub>	(130) <sub>Al</sub>    (100) <sub>β''</sub>	Pre-β''	44	Y	Y	10	18
A <sub>1</sub>	(130) <sub>Al</sub>    (100) <sub>β''</sub>	β''	88	N	N	16	6
A <sub>2</sub>	(130) <sub>Al</sub>    (100) <sub>β''</sub>	Pre-β''	88	N	N	12	9
A <sub>8</sub>	(130) <sub>Al</sub>    [100] <sub>β''</sub>	Pre-β''	88	Y	Y	10	18
B <sub>1</sub>	(001) <sub>Al</sub>    (010) <sub>β''</sub>	β''	88	N	Y	24	12
B <sub>2</sub>	(001) <sub>Al</sub>    (010) <sub>β''</sub>	Pre-β''	88	N	Y	34	40
C <sub>1</sub>	( $\bar{3}20$ ) <sub>Al</sub>    (001) <sub>β''</sub>	β''	88	N	N	28	6
C <sub>2</sub>	( $\bar{3}20$ ) <sub>Al</sub>    (001) <sub>β''</sub>	Pre-β''	88	N	N	32	8
C <sub>3</sub>	( $\bar{3}20$ ) <sub>Al</sub>    (001) <sub>β''</sub>	Pre-β''	88	Y	N	38	44
C <sub>4</sub>	( $\bar{3}20$ ) <sub>Al</sub>    (001) <sub>β''</sub>	Pre-β''	88	Y	Y	28	36

<sup>a</sup> C<sub>3</sub> is the only case where atom intermixing across interface is considered.

resulting structure is the so-called pre-β'' phase [12,24]. If one does not distinguish Mg and Si, the pre-β'' structure is a distorted fcc structure. This type of topological structure is often called a “superstructure of fcc” [12,24]. However, the β''-Mg<sub>5</sub>Si<sub>6</sub> is not a superstructure of fcc, and therefore there is some ambiguity about how to align the fcc α-Al CMUC to that of β''-Mg<sub>5</sub>Si<sub>6</sub>. In our calculations, two ways of aligning the atoms at the interface have been considered for each interfacial orientation. They are (i) the β'' alignment: the α-Al CMUC is positioned in a way that its corner Al atom exactly replaces the corner Mg of β''-Mg<sub>5</sub>Si<sub>6</sub>; and (ii) the pre-β'' or “fcc” alignment: relative to (i), all of the α-Al CMUC atoms are shifted by  $\mathbf{b}_{\beta''}/2$ .

### 3.1. Interfacial termination/position

Once the orientations and atom alignment have been determined, it is still necessary to determine the interfacial position of both phases on each side of the interface. In other words, we must determine where to “cut” the CMUCs and how to connect them together to construct the supercell. Our studies on the effect of interfacial termination on the interfacial energies are focused on the interfacial orientations (130)<sub>Al</sub>|| (100)<sub>β''</sub> and ( $\bar{3}20$ )<sub>Al</sub>|| (001)<sub>β''</sub>. The interfacial orientation (001)<sub>Al</sub>|| (010)<sub>β''</sub> corresponds to the small area interface at the top of the needle-shaped precipitate, which we suspect is incoherent or partially coherent, likely with a large interfacial energy; hence, we did not try to optimize the termination.

### 3.2. Supercells used in searching for the optimized interfacial termination for interfacial orientation (130)<sub>Al</sub>|| (100)<sub>β''</sub>

For searching for the low energy terminations, we have tried eight different supercells, labeled X<sub>1</sub>–X<sub>8</sub>, as illustrated

in Fig. 2 (by shifting the interfacial positions via systematically replacing the atoms on the β''-Mg<sub>5</sub>Si<sub>6</sub> side with Al atoms and compensating the α-Al side with those replaced atoms from β''-Mg<sub>5</sub>Si<sub>6</sub>). To accelerate this search, we use relatively small supercells (44 atoms) and moderately converged (“PREC = Medium”) VASP energetics for this purpose, but check the lowest energy terminations with larger supercells and more precise energetics, described below. The supercells X<sub>1</sub>–X<sub>4</sub> take the β'' alignment and the supercells X<sub>5</sub>–X<sub>8</sub> take the pre-β''/fcc alignment.

### 3.3. Supercells used in searching for the optimized interfacial termination for interfacial orientation ( $\bar{3}20$ )<sub>Al</sub>|| (001)<sub>β''</sub>

We have examined four terminations, labeled C<sub>1</sub>–C<sub>4</sub>, as illustrated in Fig. 3. C<sub>1</sub> takes the β'' alignment and all others take the pre-β''/fcc alignment. We particularly note the C<sub>3</sub> interface, which is constructed via “intermixing” atoms across the interface. Based on experimental observations for the interfacial orientation ( $\bar{3}20$ )<sub>Al</sub>|| (001)<sub>β''</sub>, Andersen et al. [11] suggested a model where some of the Si atoms in β''-Mg<sub>5</sub>Si<sub>6</sub> may occupy positions in the α-Al matrix. Via a careful examination of this model, we found that it could equivalently be reproduced by replacing 4 Mg atoms and 2 Si atoms from the β''-Mg<sub>5</sub>Si<sub>6</sub> side with 6 Al atoms. To build supercell C<sub>3</sub>, we swap 4 Mg atoms and 2 Si atoms from the β''-Mg<sub>5</sub>Si<sub>6</sub> side with 6 Al atoms from the α-Al side. We note that performing these atomic swaps only yields the atomic arrangements suggested by Andersen et al. [11] for one (i.e. IF2 shown in Fig. 3 for C<sub>3</sub>) of the two interfaces in the supercell.

### 3.4. Supercells used in calculating the interfacial energies

To obtain higher quantitative accuracy for the interfacial energies, we use larger supercells (88 atoms), as shown

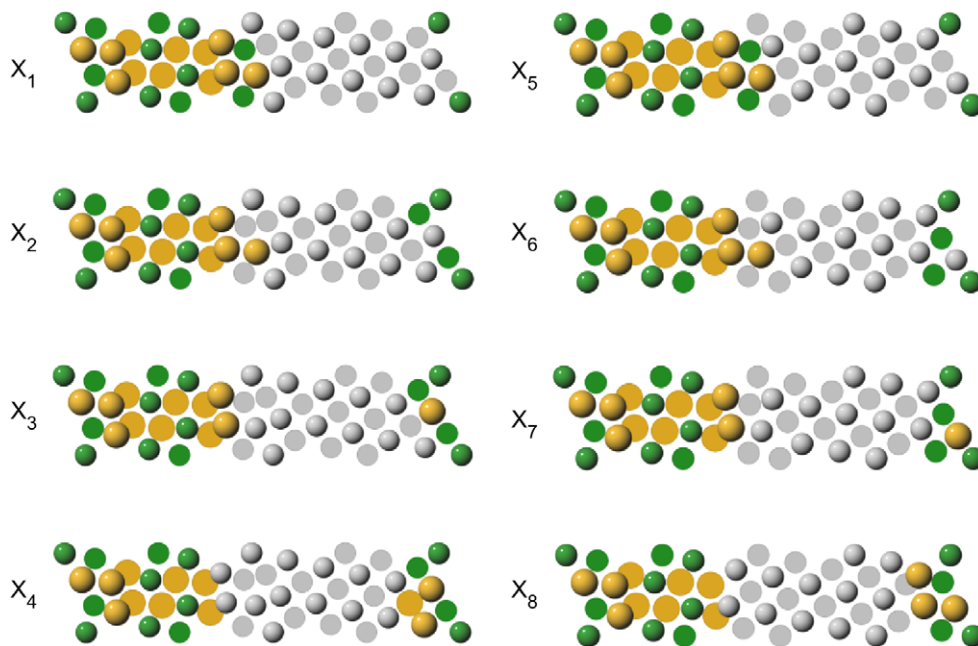


Fig. 2. Supercells used in searching for the low energy termination along orientation A  $[(1\ 30)_{\text{Al}} \parallel (1\ 00)_{\beta'}]$ . Mg: green (small balls); Si: orange (large balls); Al: gray.  $X_1$ – $X_4$  take the  $\beta'$  alignment and  $X_5$ – $X_8$  take the pre- $\beta'$ /fcc alignment. (For interpretation of the references to colour in this figure legend, the reader is referred to the web version of this article.)

in Figs. 3–5. We performed calculations on supercells for all three interfacial orientations described above:  $(\bar{3}20)_{\text{Al}} \parallel (001)_{\beta'}$  (needle- $\parallel$ , denoted by  $C_1$ ,  $C_2$ ,  $C_3$ , and  $C_4$  in Fig. 3),  $(130)_{\text{Al}} \parallel (100)_{\beta'}$  (needle- $\parallel$ , denoted by  $A_1$ ,  $A_2$  and  $A_8$  in Fig. 4) and  $(001)_{\text{Al}} \parallel (010)_{\beta'}$  (needle- $\perp$ , denoted by  $B_1$  and  $B_2$  in Fig. 5). Considering various interfacial alignments, solute intermixing configurations, and terminations, we have constructed a total of nine interfacial supercells having 88 atoms, listed as  $A_1$ ,  $A_2$ ,  $A_8$ ,  $B_1$ ,  $B_2$ ,  $C_1$ ,  $C_2$ ,  $C_3$  and  $C_4$ . Among these supercells,  $A_1$  is a cell-doubled version of supercell  $X_1$  and  $A_8$  is a cell-doubled version of supercell  $X_8$ .

### 3.5. Equivalency of the two interfaces in one supercell

Due to periodic boundary conditions, the constructed supercell always contains two interfaces. The two interfaces are either equivalent to one another or are not, depending on the symmetry dictated by the termination of the crystals. Fig. 6 is used to examine the local symmetry of  $\beta'$ - $\text{Mg}_5\text{Si}_6$ . We note two special planes: the first is marked with  $(\bar{3}20)_{\text{Al}} \parallel (001)_{\beta'}$  and the second is marked with  $(130)_{\text{Al}} \parallel (100)_{\beta'}$ . If the  $\beta'$ - $\text{Mg}_5\text{Si}_6$  CMUC is cut along one of these two planes, the two resulting surfaces are equivalent by symmetry (the intersection of these two planes yields an axis which contains an inversion center).

In our supercell models,  $X_8$ ,  $A_8$ ,  $B_1$ ,  $B_2$  and  $C_4$  contain two equivalent interfaces (marked as IF1 and IF2 in Figs. 3–5). For  $X_8$ ,  $A_8$  and  $C_4$ , the equivalency of the two interfaces is associated with the symmetry analysis of Fig. 6. For  $B_1$  and  $B_2$ , the equivalency can be observed by noting

the fact that the 11-atom layer arrangements of the pure phases along the crystal orientation  $[001]_{\text{Al}} \parallel [010]_{\beta'}$  are a simple  $ABAB$  ( $B = A + \mathbf{b}_{\beta'}/2$ ) type stacking of layers, and the interface  $B_{\text{Al}}A_{\beta'}$  is equivalent to the interface  $B_{\beta'}A_{\text{Al}}$ .

For the rest of the supercells employed in this work, the two interfaces, IF1 and IF2, contained in one supercell are not equivalent. The calculated interfacial energies are therefore the averaged values between the two interfaces. The use of non-equivalent interfaces is to preserve the stoichiometry of  $\beta'$ - $\text{Mg}_5\text{Si}_6$ , and is simply due to the symmetry and crystal structure of the  $\beta'$ - $\text{Mg}_5\text{Si}_6$  phase. For insulators, the use of non-equivalent interfaces can result in charge transfer around an interface [25] (e.g. from the matrix to the precipitate) or between the two interfaces, which can create an interface dipole. In surface calculations this situation is sometimes rectified by imposing an external dipole field [26]. However, we assume that in metallic systems the long-range dipole–dipole interaction will be screened out much more efficiently than in insulators. Other solutions to the problem of two non-equivalent interfaces dictated by stoichiometric concerns are possible, via the use of chemical potentials [27,28]. However, our calculated results (see below) show that the supercells containing two equivalent interfaces give quite low interfacial energies. In comparison, the calculated interfacial energies using supercells containing two non-equivalent interfaces are quite high. Hence, we take the supercells with equivalent interfaces as a good description of the preferred interfaces in this system, and do not try to rectify the problem of inequivalent interfaces in our high-energy supercells.

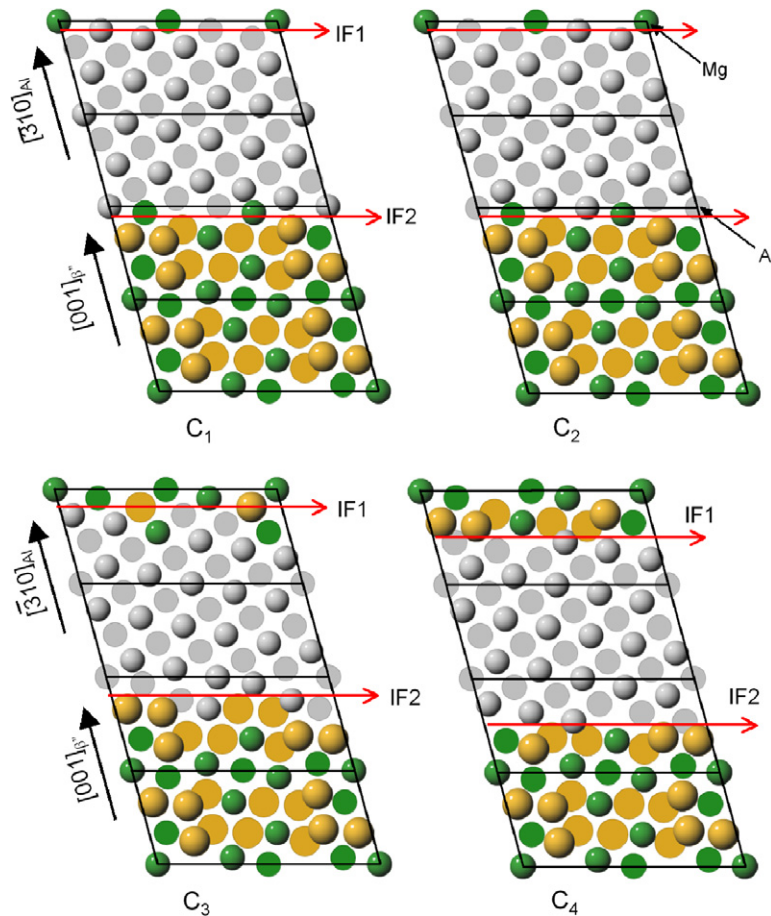


Fig. 3. Supercells used in calculating the interfacial energies along orientation C [ $(\bar{3}20)_{\text{Al}}\parallel(001)_{\beta''}$ ]. Mg: green (small balls); Si: orange (large balls); Al: gray. C<sub>1</sub>:  $\beta''$  alignment; the corner atom from matrix  $\alpha$ -Al replaces exactly the corner Mg atom position of  $\beta''$ -Mg<sub>5</sub>Si<sub>6</sub>. C<sub>2</sub>: pre- $\beta''$ /fcc alignment; relative to supercell C<sub>1</sub>, the matrix Al atoms have been shifted  $b_{\beta''}/2$ , which means the corner Al atom from matrix  $\alpha$ -Al takes back the corresponding fcc position in  $\beta''$ -Mg<sub>5</sub>Si<sub>6</sub>. C<sub>3</sub>: pre- $\beta''$ /fcc alignment; in addition to C<sub>2</sub>, 4 Mg atoms and 2 Si atoms in the  $\beta''$ -Mg<sub>5</sub>Si<sub>6</sub> side have swapped positions with the corresponding Al atoms in the  $\alpha$ -Al side. (For interpretation of the references to colour in this figure legend, the reader is referred to the web version of this article.)

#### 4. First-principles methodology

For our first-principles density functional theory calculations, we employ the Vienna ab initio simulation package (VASP) [29–31] with Vanderbilt ultrasoft pseudopotentials [32] and the generalized gradient approximation (GGA) [33]. In order to obtain highly accurate and reliable energetics, the energy cutoff is fixed to 188.3 eV, i.e. the highest energy cutoff among Al, Mg and Si suggested by VASP (using the input flag, “PREC = High”). For the pseudopotentials used, only the 3s3p orbitals are treated as valence. Unless otherwise specified, all calculations are performed including complete atomic relaxation of cell volume, cell vectors, and cell-internal atomic positions.

In the stress-free calculations for pure phases, we use a  $24 \times 24 \times 24$  Monkhorst–Pack  $\mathbf{k}$ -point grid for  $\alpha$ -Al and an  $8 \times 24 \times 16$  grid for  $\beta''$ -Mg<sub>5</sub>Si<sub>6</sub>. For the supercells with 88 atoms used in calculating the interfacial properties, two sets of  $\mathbf{k}$ -points have been used, which we generically label “coarse” and “fine”. The “coarse”  $\mathbf{k}$ -point meshes are  $2 \times 14 \times 7$ ,  $5 \times 4 \times 11$  and  $5 \times 17 \times 3$  Monkhorst–Pack

$\mathbf{k}$ -points for the interfacial orientation  $(130)_{\text{Al}}\parallel(100)_{\beta''}$ ,  $(001)_{\text{Al}}\parallel(010)_{\beta''}$  and  $(320)_{\text{Al}}\parallel(001)_{\beta''}$ , respectively. The “fine”  $\mathbf{k}$ -point meshes are  $2 \times 24 \times 16$ ,  $8 \times 6 \times 16$  and  $8 \times 24 \times 4$  gamma-centered  $\mathbf{k}$ -points for interfacial orientations  $(130)_{\text{Al}}\parallel(100)_{\beta''}$ ,  $(001)_{\text{Al}}\parallel(010)_{\beta''}$  and  $(320)_{\text{Al}}\parallel(001)_{\beta''}$ , respectively. The “fine”  $\mathbf{k}$ -point is more “shape-matched” for the various supercell shapes, i.e. closer to  $a^*k_a \equiv b^*k_b \equiv c^*k_c$  ( $k_a$ ,  $k_b$  and  $k_c$  represent the number of  $\mathbf{k}$ -points, respectively, along the three directions of lattice vectors,  $\mathbf{a}_{\beta''}$ ,  $\mathbf{b}_{\beta''}$  and  $\mathbf{c}_{\beta''}$ ). We have used the “fine”  $\mathbf{k}$ -point to refine atomically relaxed structures from the “coarse” sets, as well as to check the convergence of the “coarse” set. For the supercells with 44 atoms used to search for low-energy terminations for the interfacial orientation  $(130)_{\text{Al}}\parallel(100)_{\beta''}$ , we used a  $3 \times 17 \times 11$  Monkhorst–Pack  $\mathbf{k}$ -point mesh.

#### 5. Separation of interfacial and strain energies from first-principles supercell results

The formation energy of our supercells is defined as the energy difference between that of the supercell (containing

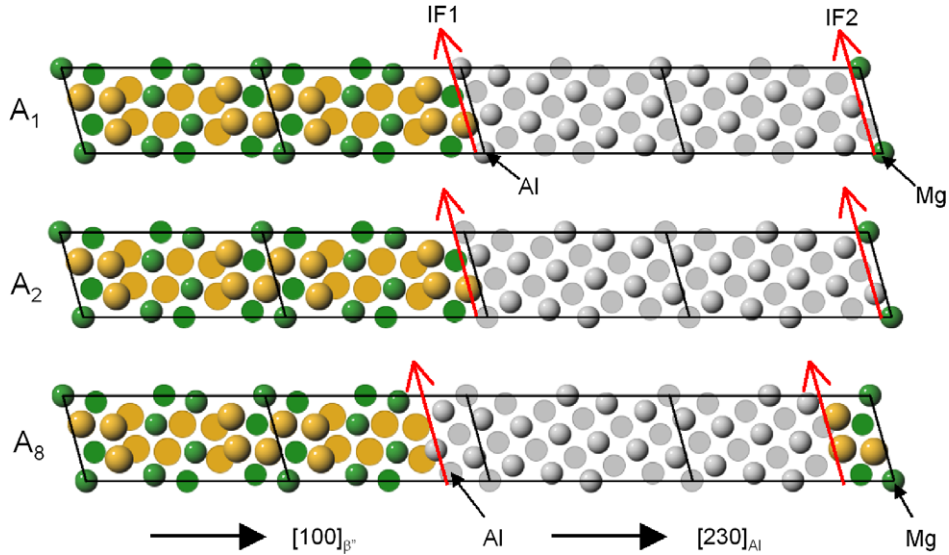


Fig. 4. Supercells used in calculating the interfacial energies along orientation A  $[(130)_{\text{Al}} \parallel (100)_{\beta'}]$ . Mg: green (small balls); Si: orange (large balls); Al: gray. A<sub>1</sub>:  $\beta'$  alignment; the corner Mg atom of  $\beta'$ -Mg<sub>5</sub>Si<sub>6</sub> is replaced by Al. A<sub>2</sub>: pre- $\beta'$ /fcc alignment; relative to supercell A<sub>1</sub>, the matrix Al atoms have been shifted  $b_{\beta'}/2$ , which means the corner Al atom from matrix  $\alpha$ -Al takes back the correspondent fcc position in  $\beta'$ -Mg<sub>5</sub>Si<sub>6</sub>. A<sub>8</sub>: pre- $\beta'$ /fcc alignment; relative to supercell A<sub>2</sub>, the interfacial position has been moved so that the bonds at the interfaces are formed by Al-Si. (For interpretation of the references to colour in this figure legend, the reader is referred to the web version of this article.)

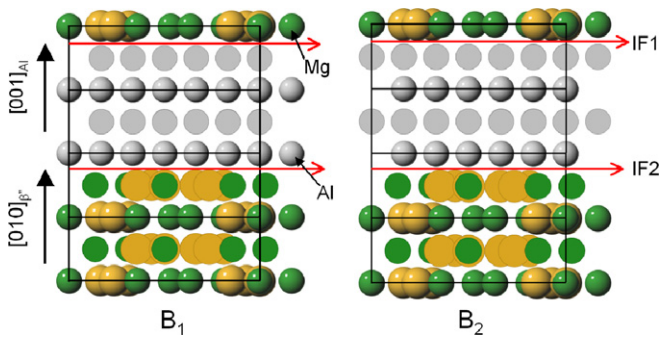


Fig. 5. Supercells used in calculating the interfacial energies along orientation B  $((010)$  crystal plane of  $\beta'$ ,  $(001)_{\text{Al}} \parallel (010)_{\beta'}$ ). Mg: green (small balls); Si: orange (large balls); Al: gray. B<sub>1</sub>:  $\beta'$  alignment; the corner atom from matrix  $\alpha$ -Al replaces exactly the corner Mg atom position of  $\beta'$ -Mg<sub>5</sub>Si<sub>6</sub>. B<sub>2</sub>: pre- $\beta'$ /fcc alignment; relative to supercell B<sub>1</sub>, the matrix Al atoms at 0 and 1/2 in the  $b_{\beta'}$  direction have switched their positions. (For interpretation of the references to colour in this figure legend, the reader is referred to the web version of this article.)

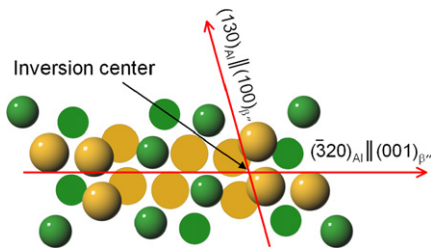


Fig. 6. Crystal structure of  $\beta'$ -Mg<sub>5</sub>Si<sub>6</sub>, showing the axis containing the inversion center, and the two planes where the crystal can be cut to obtain two equivalent interfaces in the supercells.

the interface) and the energy of the pure “constituents”,  $\alpha$ -Al or  $\beta'$ -Mg<sub>5</sub>Si<sub>6</sub>. However, this energy difference contains not only the interfacial energy, but also the coherency

strain energy required to deform the constituents from their stress-free states. To reliably extract the interfacial energy, one must separate the contribution of coherency strain. The separation procedure is described below.

### 5.1. Energies of formation

We begin with the formula for the energy of formation of an interfacial supercell. Using  $A$  and  $B$  to represent  $\alpha$ -Al and  $\beta'$ -Mg<sub>5</sub>Si<sub>6</sub>, respectively, the energy of formation,  $E_f$ , for an interfacial supercell with  $N$  atoms is given by

$$E_f = E_{AB} - xNE_A - (1 - x)NE_B, \quad (1)$$

where  $E_{AB}$  represents the total energy of the supercell.  $x$  in Eq. (1) represents the phase fraction of A ( $x = 1 - x = 0.5$  in this work since all our supercells contain equal fractions of A and B).  $E_A$  and  $E_B$  in Eq. (1) represent the energy per atom of the fully relaxed A and B structures (stress-free), i.e. the energy is minimized with respect to volume, internal atomic positions, and cell shape or bond angles. The formation energy as defined in Eq. (1) thus contains both contributions from the interfacial energy, as well as the elastic strain energy from the lattice mismatch between A and B. Specifically, the energy of formation of Eq. (1) can be expressed as [34,35]:

$$\frac{E_f}{N} = \frac{2S\sigma}{N} + \zeta \quad (2)$$

where  $S$  represents the area of the interface,  $\sigma$  is the interfacial energy per unit area and  $\zeta$  is the strain energy per atom. (The factor of two is due to the fact that there are two interfaces per supercell.)

## 5.2. Separation of interfacial energy from strain energy

For a completely coherent interface, the strain energy plays a crucial role since it is proportional to the total volume, whereas the interfacial energy is only proportional to the cross-sectional area of the supercell. There are two approaches to separate these two contributions, linear fitting and direct calculations.

**Linear fitting:** One way to extract the interfacial/strain energy from the supercell formation energy of Eq. (1) is to calculate energetics for a series of supercells with increasing size  $N$ , then fit these energetics to the expression of Eq. (2), which is linear in  $1/N$  [34,35]. In Eq. (2), it is assumed that the elastic deformations of A and B in the supercells are constant as the size of the supercells increases. Therefore, by fitting a series of calculated values of  $E_f$  versus the inverse of the supercell size,  $1/N$ , one can extract the interfacial energy from the slope of the fitted line, and the  $y$ -intercept gives the strain energy [35].

Though this method is quite straightforward in principle, it can be computationally demanding in practice as it requires a series of increasingly larger supercell calculations. For the interfacial system between  $\beta''$ -Mg<sub>5</sub>Si<sub>6</sub> and  $\alpha$ -Al in the present work, the smallest supercell consists of 44 atoms. Due to the complexity of the system, we found this linear fitting method to be computationally prohibitive.

**Direct calculation:** We can illustrate an alternative, direct method of separating strain and interfacial energies via the following imaginary two-step process: first, both the bulk crystal structures of the precipitate and the matrix are individually deformed (but not brought together) from their stress-free states to their stressed states in the interfacial geometry. That is, the two lattice vectors along the interfacial plane are strained to match one another while the supercells are allowed to relax along the direction of the third lattice vector. The energy difference between this deformed state and the stress-free state gives the strain energy upon forming a coherent interface. Second, the two perfect crystals are then broken along the interfacial orientation plane and joined together to form an interface. The energy associated with this second process corresponds to the interfacial energy. Specifically, in this work, we carried out the separation of interfacial energy and elastic strain energy using the following process:

(1) Assuming the interface is along the plane containing both lattice vector  $\mathbf{b}$  and lattice vector  $\mathbf{c}$ , we first calculate the total energy of the interface supercell with full atomic and cell-vector relaxations. The obtained total energy is denoted as  $E_{\text{Al}/\beta''}(\mathbf{a}, \mathbf{b}, \mathbf{c})$  with  $\mathbf{a}$ ,  $\mathbf{b}$  and  $\mathbf{c}$  representing the relaxed lattice vectors.

(2) We then adopt a supercell with the same shape and number of atoms as step 1, but consisting of either pure  $\alpha$ -Al or pure  $\beta''$ -Mg<sub>5</sub>Si<sub>6</sub>, but not both. (We also use the same  $\mathbf{k}$ -point and energy cutoff as in step 1.) We then fix the two lattice vectors,  $\mathbf{b}$  and  $\mathbf{c}$ , which lie in the interfacial plane of step 1, as well as the monoclinic angle, while relax-

ing the cell only along the direction of lattice vector  $\mathbf{a}$ . For the  $\beta''$ -Mg<sub>5</sub>Si<sub>6</sub> phase, we also relax all cell-internal atomic positions (for  $\alpha$ -Al, there are no cell-internal degrees of freedom by symmetry). The total energies obtained for the constrained  $\alpha$ -Al and  $\beta''$ -Mg<sub>5</sub>Si<sub>6</sub> are labeled  $E_{\text{Al}}(\mathbf{a})$  and  $E_{\beta''}(\mathbf{a})$ . The interfacial energy is then calculated as

$$\sigma = \left\{ E_{\text{Al}/\beta''}(\mathbf{a}, \mathbf{b}, \mathbf{c}) - \frac{1}{2} [E_{\text{Al}}(\mathbf{a}) + E_{\beta''}(\mathbf{a})] \right\} / 2S \quad (3)$$

where again, the factor 2 in the denominator arises from the fact that the use of periodic boundary conditions results in two interfaces in the supercell. Once the interfacial energy,  $\sigma$ , is obtained using Eq. (3), the strain energy can be obtained through Eq. (2) using  $E_f$  calculated by means of Eq. (1).

## 6. Results and discussion

### 6.1. Convergence with respect to $\mathbf{k}$ -points

We begin the discussion of our results with an analysis of the convergence of the calculations with respect to the  $\mathbf{k}$ -points. For four selected supercells, i.e. A<sub>1</sub>, B<sub>1</sub>, B<sub>2</sub> and C<sub>3</sub>, we have studied the effect of the  $\mathbf{k}$ -point mesh on energetic and structural properties. Table 2 gives the effects of  $\mathbf{k}$ -point mesh on the calculated energies of formation, strain energies and interfacial energies. Table 3 contains the  $\mathbf{k}$ -point convergence tests for the calculated lattice parameters, including the bond angle  $\beta$  between lattice vector  $\mathbf{a}_{\beta''}$  and  $\mathbf{c}_{\beta''}$ . It is found that the differences between the “coarse” and “fine” sets of  $\mathbf{k}$ -points are less than 2% for interfacial energies and less than 0.1% for the lattice parameters. Therefore, we conclude that the calculations are converged using either set of  $\mathbf{k}$ -points.

### 6.2. Lattice mismatch

The term “lattice mismatch” refers to the stress-free lattice parameter difference between the precipitate and the matrix. Because  $\beta''$ -Mg<sub>5</sub>Si<sub>6</sub> is a metastable phase (which even has a positive formation energy [24] within GGA), it

Table 2  
Calculated energetics for different  $\mathbf{k}$ -point meshes

Supercell	$\mathbf{k}$ -point mesh	Energy of formation (kJ mol <sup>-1</sup> )	Strain energy (kJ mol <sup>-1</sup> )	Interfacial energy (mJ m <sup>-2</sup> )
A <sub>1</sub>	2 × 7 × 14	1.98	0.82	316
A <sub>1</sub> <sup>a</sup>	2 × 16 × 24	2.05	0.90	313
B <sub>1</sub>	5 × 11 × 4	4.95	1.20	286
B <sub>1</sub> <sup>a</sup>	8 × 16 × 6	4.94	1.18	287
B <sub>2</sub>	5 × 11 × 4	4.92	0.76	321
B <sub>2</sub> <sup>a</sup>	8 × 16 × 6	4.97	0.74	327
C <sub>3</sub>	5 × 3 × 17	2.67	0.39	276
C <sub>3</sub> <sup>a</sup>	8 × 4 × 24	2.70	0.42	276

<sup>a</sup> Refined calculations using denser  $\mathbf{k}$ -point meshes.

Table 3  
Calculated lattice parameters for different k-point meshes

Supercell	<i>a</i> (nm)	<i>b</i> (nm)	<i>c</i> (nm)	$\beta$ (°) <sup>a</sup>
Al <sup>b</sup>	1.459	0.4047	0.6398	105.3
Expt. <sup>c</sup>	1.460	0.4050	0.6403	105.3
$\beta''$	1.512	0.4084	0.6928	110.5
Expt. <sup>d</sup>	1.516	0.405	0.674	105.3
A <sub>1</sub>	1.487 × 4	0.4061	0.6624	104.8
A <sub>1</sub> <sup>e</sup>	1.485 × 4	0.4070	0.6615	104.8
B <sub>1</sub>	1.506	0.4208 × 4	0.6813	110.9
B <sub>1</sub> <sup>e</sup>	1.505	0.4210 × 4	0.6809	110.8
B <sub>2</sub>	1.495	0.4101 × 4	0.6667	108.2
B <sub>2</sub> <sup>e</sup>	1.490	0.4116 × 4	0.6647	107.7
C <sub>3</sub>	1.497	0.4024	0.6703 × 4	107.5
C <sub>3</sub> <sup>e</sup>	1.497	0.4022	0.6703 × 4	107.5

<sup>a</sup> Angle between the lattice vectors  $\mathbf{a}_{\beta''}$  and  $\mathbf{c}_{\beta''}$ .

<sup>b</sup> Lattice parameters of  $\alpha$ -Al when the 22-atom monoclinic  $\beta''$ -Mg<sub>5</sub>Si<sub>6</sub> supercell is adopted (see text).

<sup>c</sup> These numbers are deduced based on the experimental values for pure  $\alpha$ -Al [36].

<sup>d</sup> The experimental values for constrained  $\beta''$ -Mg<sub>5</sub>Si<sub>6</sub> precipitate [12] in an  $\alpha$ -Al matrix.

<sup>e</sup> Refined calculations using denser k-point mesh.

is virtually impossible to experimentally obtain a bulk crystal of  $\beta''$ -Mg<sub>5</sub>Si<sub>6</sub>, and thereby to observe the stress-free lattice parameters of  $\beta''$ -Mg<sub>5</sub>Si<sub>6</sub>. But, from our first-principles calculations, we can compute quantitative values of the lattice mismatch.

For pure  $\alpha$ -Al, our calculated fcc lattice constant is 0.4047 nm, which is almost identical to the measured room temperature value of 0.405 nm [36]. For  $\beta''$ -Mg<sub>5</sub>Si<sub>6</sub>, our stress-free calculated lattice constants are  $a_{\beta''} = 1.5118$  nm,  $b_{\beta''} = 0.4084$  nm and  $c_{\beta''} = 0.6928$  nm. From these data, the deduced theoretical lattice mismatches between  $\alpha$ -Al and  $\beta''$ -Mg<sub>5</sub>Si<sub>6</sub> are +3.6%, +0.9% and +8.3%, respectively, along the three lattice directions  $\mathbf{a}_{\beta''}$ ,  $\mathbf{b}_{\beta''}$  and  $\mathbf{c}_{\beta''}$ . It is interesting to note that the direction in which the  $\beta''$ -Mg<sub>5</sub>Si<sub>6</sub> precipitates are observed to be fully coherent (along the  $\mathbf{b}_{\beta''}$  axis) is the lattice constant predicted by first-principles to have the lowest lattice mismatch.

### 6.3. Effects of supercell size

For supercells with periodic boundary conditions, the interaction between the periodic images of the supercell could affect both the interfacial energy and strain energy, as well as the structural properties. As an example, we discuss the effect of supercell size on the interfacial energies for the orientation (130)<sub>Al</sub>|| (100) <sub>$\beta''$</sub> . We compare a 44-atom supercell X<sub>1</sub> with a 88-atom supercell A<sub>1</sub> and a 44-atom supercell X<sub>8</sub> with a 88-atom supercell A<sub>8</sub>.

Supercells X<sub>1</sub> and A<sub>1</sub> have the  $\beta''$  alignment. If a supercell is sufficiently large, the calculated interfacial energy should not be dependent on the supercell size. However, a comparison between X<sub>1</sub> and A<sub>1</sub> demonstrates significant differences in the calculated interfacial energy and strain

energy. As the supercell is doubled, the strain energy per mol atom is decreased while the interfacial energy is increased (see Table 4). The decrease in the strain energy per mol atom can be understood by the change of bond angle  $\beta$  listed in Table 5 from supercells X<sub>1</sub> (102.3°) to A<sub>1</sub> (104.8°). The bond angle  $\beta = 102.3^\circ$  for supercell X<sub>1</sub> is quite small compared with the pure phases (110.5° for  $\beta''$ -Mg<sub>5</sub>Si<sub>6</sub> and 105.3° for  $\alpha$ -Al).

On the other hand, supercells X<sub>8</sub> and A<sub>8</sub> have the pre- $\beta''$ /fcc alignment. In contrast to the comparison between X<sub>1</sub> and A<sub>1</sub>, comparison between X<sub>8</sub> and A<sub>8</sub> shows very little size effect, as can be seen in Tables 4 and 5. The interfacial energy, strain energy, bond angle  $\beta$  and in-plane lattice parameters (see Table 5) are roughly unchanged as the supercell is doubled from X<sub>8</sub> to A<sub>8</sub>.

### 6.4. Interfacial energies

The calculated energies of formation, strain (elastic) energies and interfacial energies are summarized for all supercells in Table 4. There is quite a strong variation in interfacial energies for the supercells considered, with the

Table 4  
First-principles calculated energetics for the different  $\beta''$ -Mg<sub>5</sub>Si<sub>6</sub>/ $\alpha$ -Al interfacial supercells

Supercell	Energy of formation (kJ mol <sup>-1</sup> )	Strain energy (kJ mol <sup>-1</sup> )	Interfacial energy (mJ m <sup>-2</sup> )
X <sub>1</sub>	3.45	1.61	251
X <sub>8</sub>	1.54	0.65	123
A <sub>1</sub>	1.98	0.82	316
A <sub>2</sub>	2.19	0.55	449
A <sub>8</sub>	1.06	0.61	124
B <sub>1</sub>	4.95	1.20	286
B <sub>2</sub>	4.92	0.76	321
C <sub>1</sub>	3.64	0.70	361
C <sub>2</sub>	3.78	0.62	392
C <sub>3</sub>	2.67	0.39	276
C <sub>4</sub>	1.27	0.45	100

Table 5  
First-principles calculated lattice parameters for the different  $\beta''$ -Mg<sub>5</sub>Si<sub>6</sub>/ $\alpha$ -Al interfacial supercells<sup>a</sup>

Supercell	<i>a</i> (nm)	<i>b</i> (nm)	<i>c</i> (nm)	$\beta$ (°)
X <sub>1</sub>	1.4950 × 2	0.4068	0.6588	102.3
X <sub>8</sub>	1.498 × 2	0.4040	0.6568	106.2
A <sub>1</sub>	1.487 × 4	0.4061	0.6624	104.8
A <sub>2</sub>	1.514 × 4	0.4035	0.6603	107.1
A <sub>8</sub>	1.494 × 4	0.4046	0.6591	106.5
B <sub>1</sub>	1.506	0.4208 × 4	0.6813	110.9
B <sub>2</sub>	1.495	0.4101 × 4	0.6667	108.2
C <sub>1</sub>	1.477	0.4029	0.6958 × 4	105.3
C <sub>2</sub>	1.481	0.3977	0.7038 × 4	108.0
C <sub>3</sub>	1.497	0.4024	0.6703 × 4	107.5
C <sub>4</sub>	1.483	0.4052	0.6651 × 4	106.8

<sup>a</sup> See Table 2 for an explanation of the various lattice parameters.

difference between the highest and lowest interfacial energies of about a factor of  $\sim 3$ . In general, the supercells containing two equivalent interfaces are lower in energy. For the experimentally observed interfaces (needle- $\parallel$ ),  $(\bar{3}20)_{\text{Al}}\parallel(001)_{\beta''}$  and  $(130)_{\text{Al}}\parallel(100)_{\beta''}$ , the lowest calculated interfacial energies are 100 and 124  $\text{mJ m}^{-2}$  from cells  $C_4$  and  $A_8$ , respectively. In contrast, the calculated interfacial energies at the needle top,  $(001)_{\text{Al}}\parallel(010)_{\beta''}$  (needle- $\perp$ ), are much larger, on the order of  $\sim 300 \text{ mJ m}^{-2}$ . The calculated strain energy for the two needle- $\parallel$  interfaces is 0.61  $\text{kJ mol}^{-1}$  for  $A_8$  and 0.45  $\text{kJ mol}^{-1}$  for  $C_4$ , which are also lower than those for the needle- $\perp$  interface calculated through  $B_1$  and  $B_2$ .

Two of the important factors that determine the interfacial energy of an interface are the interfacial alignment and interfacial termination. Our results indicate that the pre- $\beta''$ /fcc alignment as well as maximizing the difference between the number of Al–Si bonds and the number of Al–Mg bonds both lead to both low interfacial energies and low strain energies. From Tables 1 and 4 one can find that all of the low strain energy supercells, i.e.  $X_8$ ,  $A_2$ ,  $A_8$ ,  $B_2$ ,  $C_2$ ,  $C_3$  and  $C_4$ , have the pre- $\beta''$ /fcc alignment. For all the  $(130)_{\text{Al}}\parallel(100)_{\beta''}$  interfaces considered, the lowest energy supercell  $A_8$  contains the highest difference between the number of Al–Si bonds and the number of Al–Mg bonds. Similarly, for all the  $(\bar{3}20)_{\text{Al}}\parallel(001)_{\beta''}$  interfaces, the one ( $C_4$ ) with the largest difference between the number of Al–Si bonds and the number of Al–Mg bonds results in the lowest interfacial energy. To make these arguments more quantitative, we also list the number of Al–Mg and Al–Si bonds across the interface for each of the supercell considered in Table 1. Recent first-principles calculations of Mg, Si and other impurities in  $\alpha$ -Al by Wolverton and Ozolins [37] also showed a similar ordering tendency of Al–Si bonds relative to Al–Mg bonds in the fcc geometry. With respect to the fcc lattice, they found that Si impurities in Al have negative formation energies while Mg impurities have positive formation energies. These ordering tendencies from bulk impurities are consistent with the interfacial ordering tendencies deduce in the present work.

Next, we discuss the results in more detail below for each of the three specific interfacial orientations.

*Interfacial orientation  $(130)_{\text{Al}}\parallel(100)_{\beta''}$ :* for this interfacial orientation, we have considered eight supercells with 44 atoms, labeled  $X_1$ – $X_8$ , and three supercells having 88 atoms, labeled  $A_1$ ,  $A_2$  and  $A_8$ . The small supercells  $X_1$ – $X_8$  are adopted for the purpose of searching for the low energy interfacial termination/position. Note that the only difference between  $A_2$  and  $A_8$  is the interfacial position, where the  $A_8$  supercell contains an enhanced number of Al–Si bonds across the interface. Of all these terminations, we find that supercells  $X_8$  and  $A_8$  give the lowest interfacial energy, of  $\sim 124 \text{ mJ m}^{-2}$ . Supercell  $A_2$  leads to the highest interfacial energy, of  $\sim 449 \text{ mJ m}^{-2}$ .

Even though interface  $A_8$  is energetically preferred, it is still interesting to compare the energies for cells  $A_2$  and  $A_1$ ,

since the difference between these cells lies solely in the interfacial alignment. The division of formation energy into strain and interfacial contributions is quite different in the two cases: the supercell  $A_1$  has lower interfacial energy while the supercell  $A_2$  has lower strain energy (see Table 4). The difference in strain energy between supercell  $A_1$  and supercell  $A_2$  can be understood by the supercell shape changes; for example, the bond angle  $\beta$  is found to be changed from  $104.8^\circ$  to  $107.1^\circ$  between supercell  $A_1$  and supercell  $A_2$  (see Table 5). The supercell shape changes from  $A_1$  to  $A_2$  demonstrate the effects of interfacial alignment.

*Interfacial orientation  $(001)_{\text{Al}}\parallel(01,0)_{\beta''}$ :* this interfacial orientation corresponds to the observed interface for the small area between the needle top of  $\beta''$ - $\text{Mg}_5\text{Si}_6$  precipitate and  $\alpha$ -Al. Thus, from the observed needle-shaped morphologies of  $\beta''$  precipitates, one might expect that this interfacial orientation should have a substantially larger interfacial or strain energy (or both) than the other two. Indeed, this interfacial orientation gives (Table 4) formation energies that are quite high compared with the formation energy from interfacial orientation  $(\bar{3}20)_{\text{Al}}\parallel(001)_{\beta''}$  or  $(130)_{\text{Al}}\parallel(100)_{\beta''}$ . The pre- $\beta''$ /fcc alignment seems to offer some lowering of the strain energy relative to the  $\beta''$  alignment, but at the expense of a higher interfacial energy. We also note that the observed precipitate lattice parameters indicate that this interface is not coherent, whereas our calculations correspond to a coherent interface. Breaking coherency with the lattice for this interface would likely reduce the strain energy, at the expense of an increase in the interfacial energies. Thus, we suggest that our calculated energies for coherent  $(001)_{\text{Al}}\parallel(010)_{\beta''}$  interface represent an upper bound to the true strain energy and a lower bound to the true interfacial energy.

*Interfacial orientation  $(\bar{3}20)_{\text{Al}}\parallel(001)_{\beta''}$ :* we have four supercells for this interfacial orientation,  $C_1$ ,  $C_2$ ,  $C_3$  and  $C_4$ , as listed in Table 4. As mentioned above, the  $C_2$  is different from  $C_1$  only in the interfacial alignment, while in  $C_3$ , we have swapped the positions of six pairs of atoms relative to  $C_2$ . We note that  $C_4$  contains the largest difference between Al–Si and Al–Mg bonds and also contains two equivalent interfaces.

Just as found for the other two interfacial orientations, in going from  $\beta''$  to pre- $\beta''$ /fcc alignment ( $C_1$  to  $C_2$ ), the strain energy is decreased slightly while the interfacial energy is increased slightly. However, these effects compensate one another to a great extent, giving similar formation energies. On the other hand, supercell  $C_3$  with solute intermixing across the interface results in relatively lower interfacial energy and significantly lower strain energy when compared with  $C_1$  or  $C_2$ . To a certain extent, our results for  $C_3$  support the experimental results of Andersen et al. [11], that the atomic position intermixing near the interface plays a role in the energetically preferred interfacial geometry. However, we reiterate that only one of the two interfaces (IF2) in supercell  $C_3$  is equal to the model proposed by Andersen et al. [11], and thus the calculated interfacial

energy in Table 4 represents the average of the interfacial energies of IF1 and IF2.

The most meaningful results are from C<sub>4</sub>. C<sub>4</sub> produces a surprisingly low interfacial energy of 100 mJ m<sup>-2</sup>, while its strain energy is also lower than that of the energetically preferred A<sub>8</sub> for the interfacial orientation (130)<sub>Al</sub>|| (100)<sub>β''</sub>. The value of 100 mJ m<sup>-2</sup> for C<sub>4</sub> and the value of 124 mJ m<sup>-2</sup> for A<sub>8</sub> are even lower than the calculated interfacial energy of 170 mJ m<sup>-2</sup> for the coherent interface of θ'-Al<sub>2</sub>Cu precipitates in α-Al [21,35]. We note that the energetically preferred terminations C<sub>4</sub> and A<sub>8</sub> both have the fcc topological alignment of atoms across the interfaces and have a large number of Al–Si bonds. We suspect that if one could intermix the atoms at interface IF1 in C<sub>3</sub> to also yield a larger number of Al–Si bonds, we might reduce the calculated interfacial energy for C<sub>3</sub> even further, perhaps even down to the value similar to those of C<sub>4</sub> and A<sub>8</sub>.

### 6.5. Relaxed atomic coordinates

To help interested readers in reconstructing our interfacial supercells, we give in Tables A1–A5 of the Appendix the relaxed atomic coordinates, nearest neighboring atom coordination and bond distances for the low-energy supercells A<sub>8</sub>, C<sub>4</sub> and C<sub>3</sub>, as well as B<sub>1</sub> and B<sub>2</sub>.

## 7. Summary

We have calculated interfacial energies, strain energies and lattice mismatches for the interfacial system β''-Mg<sub>5</sub>Si<sub>6</sub>/α-Al. Our study involved three types of interfacial orientations between β''-Mg<sub>5</sub>Si<sub>6</sub> and α-Al, namely, (130)<sub>Al</sub>|| (100)<sub>β''</sub>, (001)<sub>Al</sub>|| (010)<sub>β''</sub> and (320)<sub>Al</sub>|| (001)<sub>β''</sub>. In each case, we find that the low-energy interfaces possess two key attributes in common: a large number of Al–Si bonds and an alignment across the interface with a pre-β''/fcc topology.

The calculated interfacial energies for these three interfacial orientations are in the range 100–449 mJ m<sup>-2</sup>, with low energies occurring for two interfacial orientations, (320)<sub>Al</sub>|| (001)<sub>β''</sub> and (130)<sub>Al</sub>|| (100)<sub>β''</sub>, and a relatively high energy for interfacial orientation (001)<sub>Al</sub>|| (010)<sub>β''</sub>. For interfaces with interfacial orientations (320)<sub>Al</sub>|| (001)<sub>β''</sub> and (130)<sub>Al</sub>|| (100)<sub>β''</sub>, the lowest energies are found for the terminations chosen so as to maximize the difference between the number of Al–Si bonds and the number of Al–Mg bonds across the interfaces. We believe that the formation of more Al–Si bonds is the main reason for the energy lowering.

The generic finding of two low-energy orientations and a third higher-energy orientation is consistent with the observed needle-shaped morphology of β''-Mg<sub>5</sub>Si<sub>6</sub> precipitates. However, we note that the interfacial anisotropy alone cannot explain the observed large aspect ratios of the observed needle-shaped precipitates in this system. Hence, strain and other anisotropies must be adequately accounted for in a quantitative prediction of β''-Mg<sub>5</sub>Si<sub>6</sub>

precipitate shapes. Such a quantitative study using first-principles energetics is forthcoming.

## Acknowledgements

This work is funded by the National Science Foundation (NSF) through Grant DMR-0205232. First-principles calculations were carried out on the LION clusters at the Pennsylvania State University, supported in part by the NSF Grants (DMR-9983532, DMR-0122638, and DMR-0205232) and in part by the Materials Simulation Center and the Graduate Education and Research Services at the Pennsylvania State University. This research also used resources of the National Energy Research Scientific Computing Center, which is supported by the Office of Science of the U.S. Department of Energy under Contract No. DE-AC02-05CH11231. We would also like to thank Dr. Shunli Shang in our Phases Research Lab for stimulating discussions.

## Appendix

See Tables A1–A5.

Table A1  
Atomic positions for interfacial supercell A<sub>8</sub> (see Table 5 for the calculated lattice parameters)

Index <sup>a</sup>	Symbol	Internal position			Nearest neighboring atom		
		x	y	z	Index	Bond type	Distance (nm)
2	Mg	0.2518	0.9970	0.0000	22	Mg–Si	0.259
3	Mg	0.1232	0.0030	0.5000	26	Mg–Si	0.259
1	Mg	0.9956	0.0218	0.0000	21	Mg–Si	0.262
4	Mg	0.3794	0.9782	0.5000	27	Mg–Si	0.262
9	Mg	0.4216	0.9045	0.0000	24	Mg–Si	0.277
19	Mg	0.9534	0.0955	0.5000	43	Mg–Si	0.277
7	Mg	0.2121	0.0681	0.5000	25	Mg–Si	0.280
8	Mg	0.1629	0.9319	0.0000	23	Mg–Si	0.280
16	Mg	0.4007	0.3605	0.0000	31	Mg–Si	0.280
20	Mg	0.9743	0.6395	0.5000	42	Mg–Si	0.280
5	Mg	0.0835	0.0746	0.0000	26	Mg–Si	0.281
6	Mg	0.3409	0.0604	0.0000	27	Mg–Si	0.281
10	Mg	0.0341	0.9396	0.5000	21	Mg–Si	0.281
11	Mg	0.2915	0.9254	0.5000	22	Mg–Si	0.281
14	Mg	0.2317	0.6286	0.5000	22	Mg–Si	0.286
15	Mg	0.1433	0.3714	0.0000	26	Mg–Si	0.286
12	Mg	0.1029	0.6344	0.0000	23	Mg–Si	0.287
13	Mg	0.3609	0.6168	0.0000	27	Mg–Si	0.287
17	Mg	0.0141	0.3832	0.5000	21	Mg–Si	0.287
18	Mg	0.2721	0.3656	0.5000	25	Mg–Si	0.287
22	Si	0.2664	0.6625	0.0000	25	Si–Si	0.238
23	Si	0.1379	0.6691	0.5000	26	Si–Si	0.238
25	Si	0.2371	0.3309	0.0000	22	Si–Si	0.238
26	Si	0.1086	0.3375	0.5000	23	Si–Si	0.238
21	Si	0.0090	0.6760	0.0000	35	Si–Si	0.239
27	Si	0.3660	0.3240	0.5000	41	Si–Si	0.239
35	Si	0.0479	0.6447	0.0000	21	Si–Si	0.239
36	Si	0.3052	0.6294	0.0000	22	Si–Si	0.239
37	Si	0.1767	0.6365	0.5000	23	Si–Si	0.239
39	Si	0.1983	0.3635	0.0000	25	Si–Si	0.239
40	Si	0.0698	0.3706	0.5000	26	Si–Si	0.239

(continued on next page)

Table A1 (continued)

Index <sup>a</sup>	Symbol	Internal position			Nearest neighboring atom		
		x	y	z	Index	Bond type	Distance (nm)
41	Si	0.3271	0.3553	0.5000	27	Si–Si	0.239
24	Si	0.3969	0.6501	0.5000	27	Si–Si	0.240
43	Si	0.9781	0.3499	0.0000	21	Si–Si	0.240
28	Si	0.0447	0.2649	0.0000	35	Si–Si	0.245
34	Si	0.3303	0.7351	0.5000	41	Si–Si	0.245
29	Si	0.3015	0.2460	0.0000	36	Si–Si	0.247
30	Si	0.1729	0.2541	0.5000	37	Si–Si	0.247
32	Si	0.2021	0.7459	0.0000	39	Si–Si	0.247
33	Si	0.0735	0.7540	0.5000	40	Si–Si	0.247
38	Si	0.4396	0.6373	0.5000	24	Si–Si	0.258
44	Si	0.9354	0.3627	0.0000	43	Si–Si	0.258
60	Al	0.8804	0.7212	0.5000	63	Al–Al	0.278
86	Al	0.4946	0.2788	0.0000	88	Al–Al	0.278
54	Al	0.8580	0.2642	0.5000	78	Al–Al	0.279
67	Al	0.5170	0.7358	0.0000	85	Al–Al	0.279
78	Al	0.8898	0.4402	0.0000	54	Al–Al	0.279
85	Al	0.4852	0.5598	0.5000	67	Al–Al	0.279
45	Al	0.5054	0.0027	0.5000	85	Al–Al	0.282
74	Al	0.8696	0.9973	0.0000	78	Al–Al	0.282
47	Al	0.5281	0.4592	0.5000	85	Al–Al	0.283
50	Al	0.8143	0.3588	0.5000	76	Al–Al	0.283
71	Al	0.5607	0.6412	0.0000	47	Al–Al	0.283
76	Al	0.8469	0.5408	0.0000	78	Al–Al	0.283
46	Al	0.7482	0.9972	0.5000	66	Al–Al	0.284
48	Al	0.7702	0.4509	0.5000	72	Al–Al	0.284
49	Al	0.5718	0.3683	0.5000	47	Al–Al	0.284
51	Al	0.5500	0.9154	0.5000	69	Al–Al	0.284
52	Al	0.7921	0.9042	0.5000	70	Al–Al	0.284
53	Al	0.6159	0.2764	0.5000	77	Al–Al	0.284
55	Al	0.5939	0.8227	0.5000	73	Al–Al	0.284
57	Al	0.6600	0.1824	0.5000	79	Al–Al	0.284
59	Al	0.6379	0.7296	0.5000	81	Al–Al	0.284
61	Al	0.7040	0.0905	0.5000	82	Al–Al	0.284
62	Al	0.6820	0.6364	0.5000	83	Al–Al	0.284
64	Al	0.7261	0.5440	0.5000	68	Al–Al	0.284
66	Al	0.7811	0.1773	0.0000	46	Al–Al	0.284
68	Al	0.7591	0.7236	0.0000	64	Al–Al	0.284
69	Al	0.5829	0.0958	0.0000	51	Al–Al	0.284
70	Al	0.8250	0.0846	0.0000	52	Al–Al	0.284
72	Al	0.8032	0.6317	0.0000	76	Al–Al	0.284
73	Al	0.6268	0.0028	0.0000	55	Al–Al	0.284
75	Al	0.6048	0.5491	0.0000	49	Al–Al	0.284
77	Al	0.6489	0.4560	0.0000	53	Al–Al	0.284
79	Al	0.6930	0.3636	0.0000	57	Al–Al	0.284
81	Al	0.6710	0.9095	0.0000	59	Al–Al	0.284
82	Al	0.7371	0.2704	0.0000	61	Al–Al	0.284
83	Al	0.7150	0.8176	0.0000	62	Al–Al	0.284
56	Al	0.8365	0.8152	0.5000	74	Al–Al	0.285
65	Al	0.5385	0.1848	0.0000	45	Al–Al	0.285
31	Si	0.4255	0.2243	0.5000	84	Si–Al	0.256
42	Si	0.9495	0.7757	0.0000	80	Si–Al	0.256
80	Al	0.9129	0.9053	0.0000	42	Al–Si	0.256
84	Al	0.4621	0.0947	0.5000	31	Al–Si	0.256
63	Al	0.9223	0.6158	0.5000	42	Al–Si	0.262
88	Al	0.4527	0.3842	0.0000	31	Al–Si	0.262
58	Al	0.9052	0.1801	0.5000	44	Al–Si	0.275
87	Al	0.4698	0.8199	0.0000	38	Al–Si	0.275

<sup>a</sup> The label “Index” is used to label the atom position.

Table A2

Atomic positions for interfacial supercell C<sub>3</sub>

Index	Symbol	Internal position			Nearest neighboring atom		
		x	y	z	Index	Bond type	Distance (nm)
2	Mg	0.0080	0.2579	0.0000	26	Mg–Si	0.270
4	Mg	0.5080	0.2579	0.5000	28	Mg–Si	0.270
1	Mg	0.0153	0.9983	0.0000	25	Mg–Si	0.271
3	Mg	0.5153	0.9983	0.5000	27	Mg–Si	0.271
11	Mg	0.4319	0.1619	0.0000	23	Mg–Si	0.278
12	Mg	0.9319	0.1619	0.5000	21	Mg–Si	0.278
13	Mg	0.5883	0.0941	0.0000	27	Mg–Si	0.279
15	Mg	0.0883	0.0941	0.5000	25	Mg–Si	0.279
5	Mg	0.3556	0.0165	0.0000	27	Mg–Si	0.282
7	Mg	0.8556	0.0165	0.5000	25	Mg–Si	0.282
9	Mg	0.6643	0.2387	0.0000	23	Mg–Si	0.283
10	Mg	0.1643	0.2387	0.5000	21	Mg–Si	0.283
14	Mg	0.5905	0.3555	0.0000	28	Mg–Si	0.284
16	Mg	0.0905	0.3555	0.5000	26	Mg–Si	0.284
19	Mg	0.1704	0.9779	0.5000	43	Mg–Si	0.286
20	Mg	0.6704	0.9779	0.0000	44	Mg–Si	0.286
6	Mg	0.3498	0.2728	0.0000	28	Mg–Si	0.289
8	Mg	0.8498	0.2728	0.5000	26	Mg–Si	0.289
21	Si	0.0639	0.1706	0.0000	35	Si–Si	0.238
23	Si	0.5639	0.1706	0.5000	37	Si–Si	0.238
35	Si	0.2167	0.1605	0.0000	21	Si–Si	0.238
37	Si	0.7167	0.1605	0.5000	23	Si–Si	0.238
25	Si	0.9554	0.0841	0.0000	39	Si–Si	0.239
27	Si	0.4554	0.0841	0.5000	41	Si–Si	0.239
39	Si	0.8028	0.0949	0.0000	25	Si–Si	0.239
41	Si	0.3028	0.0949	0.5000	27	Si–Si	0.239
26	Si	0.9526	0.3449	0.0000	40	Si–Si	0.241
28	Si	0.4526	0.3449	0.5000	42	Si–Si	0.241
40	Si	0.7953	0.3508	0.0000	26	Si–Si	0.241
42	Si	0.2953	0.3508	0.5000	28	Si–Si	0.241
29	Si	0.2053	0.0649	0.0000	41	Si–Si	0.247
30	Si	0.1988	0.3196	0.0000	42	Si–Si	0.247
31	Si	0.7053	0.0649	0.5000	39	Si–Si	0.247
32	Si	0.6988	0.3196	0.5000	40	Si–Si	0.247
33	Si	0.8155	0.1899	0.0000	37	Si–Si	0.248
34	Si	0.3155	0.1899	0.5000	35	Si–Si	0.248
22	Si	0.0434	0.4422	0.0000	26	Si–Si	0.256
24	Si	0.5434	0.4422	0.5000	28	Si–Si	0.256
36	Si	0.2030	0.4249	0.0000	22	Si–Si	0.257
38	Si	0.7030	0.4249	0.5000	24	Si–Si	0.257
63	Al	0.5600	0.9060	0.5000	67	Al–Al	0.258
72	Al	0.0600	0.9060	0.0000	76	Al–Al	0.258
45	Al	0.4118	0.3996	0.0000	77	Al–Al	0.266
46	Al	0.9118	0.3996	0.5000	51	Al–Al	0.266
51	Al	0.9833	0.5032	0.5000	46	Al–Al	0.266
77	Al	0.4833	0.5032	0.0000	45	Al–Al	0.266
87	Al	0.9465	0.8079	0.0000	72	Al–Al	0.267
88	Al	0.4465	0.8079	0.5000	63	Al–Al	0.267
54	Al	0.0889	0.8459	0.5000	72	Al–Al	0.269
81	Al	0.5889	0.8459	0.0000	63	Al–Al	0.269
52	Al	0.9939	0.7419	0.5000	54	Al–Al	0.272
78	Al	0.4939	0.7419	0.0000	81	Al–Al	0.272
53	Al	0.0792	0.6126	0.5000	57	Al–Al	0.280
57	Al	0.1762	0.7198	0.5000	53	Al–Al	0.280
65	Al	0.8150	0.7663	0.5000	87	Al–Al	0.280
66	Al	0.7186	0.6556	0.5000	60	Al–Al	0.280
68	Al	0.8993	0.6333	0.5000	64	Al–Al	0.280
74	Al	0.3150	0.7663	0.0000	88	Al–Al	0.280
75	Al	0.2186	0.6556	0.0000	69	Al–Al	0.280
79	Al	0.3993	0.6333	0.0000	73	Al–Al	0.280
80	Al	0.5792	0.6126	0.0000	84	Al–Al	0.280
84	Al	0.6762	0.7198	0.0000	80	Al–Al	0.280

Table A2 (continued)

Index	Symbol	Internal position			Nearest neighboring atom		
		x	y	z	Index	Bond type	Distance (nm)
59	Al	0.3569	0.6990	0.5000	88	Al–Al	0.282
61	Al	0.6369	0.7849	0.5000	81	Al–Al	0.282
70	Al	0.1369	0.7849	0.0000	54	Al–Al	0.282
86	Al	0.8569	0.6990	0.0000	87	Al–Al	0.282
55	Al	0.2604	0.5898	0.5000	73	Al–Al	0.283
58	Al	0.4390	0.5662	0.5000	73	Al–Al	0.283
62	Al	0.5368	0.6770	0.5000	61	Al–Al	0.283
71	Al	0.0368	0.6770	0.0000	70	Al–Al	0.283
82	Al	0.7604	0.5898	0.0000	64	Al–Al	0.283
85	Al	0.9390	0.5662	0.0000	64	Al–Al	0.283
43	Si	0.3286	0.9388	0.5000	76	Si–Al	0.258
44	Si	0.8286	0.9388	0.0000	67	Si–Al	0.258
67	Al	0.7262	0.8962	0.5000	44	Al–Si	0.258
76	Al	0.2262	0.8962	0.0000	43	Al–Si	0.258
49	Al	0.8368	0.4545	0.0000	40	Al–Si	0.266
50	Al	0.3368	0.4545	0.5000	42	Al–Si	0.266
47	Al	0.6626	0.4814	0.0000	24	Al–Si	0.268
48	Al	0.1626	0.4814	0.5000	22	Al–Si	0.268
64	Al	0.8034	0.5261	0.5000	38	Al–Si	0.268
73	Al	0.3034	0.5261	0.0000	36	Al–Si	0.268
60	Al	0.6208	0.5487	0.5000	24	Al–Si	0.274
69	Al	0.1208	0.5487	0.0000	22	Al–Si	0.274
56	Al	0.2718	0.8308	0.5000	43	Al–Si	0.276
83	Al	0.7718	0.8308	0.0000	44	Al–Si	0.276
17	Mg	0.4204	0.8935	0.0000	63	Mg–Al	0.285
18	Mg	0.9204	0.8935	0.5000	72	Mg–Al	0.285

Table A3 (continued)

Index	Symbol	Internal position			Nearest neighboring atom		
		x	y	z	Index	Bond type	Distance (nm)
39	Si	0.7053	0.1581	0.5000	23	Si–Si	0.237
41	Si	0.7947	0.0919	0.0000	25	Si–Si	0.237
43	Si	0.2947	0.0919	0.5000	27	Si–Si	0.237
22	Si	0.0683	0.9070	0.0000	38	Si–Si	0.244
24	Si	0.5683	0.9070	0.5000	40	Si–Si	0.244
26	Si	0.9317	0.3430	0.0000	42	Si–Si	0.244
28	Si	0.4317	0.3430	0.5000	44	Si–Si	0.244
38	Si	0.2255	0.8950	0.0000	22	Si–Si	0.244
40	Si	0.7255	0.8950	0.5000	24	Si–Si	0.244
42	Si	0.7745	0.3550	0.0000	26	Si–Si	0.244
44	Si	0.2745	0.3550	0.5000	28	Si–Si	0.244
29	Si	0.1983	0.0624	0.0000	43	Si–Si	0.247
31	Si	0.6983	0.0624	0.5000	41	Si–Si	0.247
33	Si	0.8017	0.1876	0.0000	39	Si–Si	0.247
35	Si	0.3017	0.1876	0.5000	37	Si–Si	0.247
30	Si	0.1787	0.3147	0.0000	44	Si–Si	0.253
32	Si	0.6787	0.3147	0.5000	42	Si–Si	0.253
34	Si	0.8213	0.9353	0.0000	40	Si–Si	0.253
36	Si	0.3213	0.9353	0.5000	38	Si–Si	0.253
45	Al	0.9972	0.5053	0.5000	66	Al–Al	0.274
46	Al	0.0028	0.7447	0.5000	48	Al–Al	0.274
75	Al	0.4972	0.5053	0.0000	78	Al–Al	0.274
76	Al	0.5028	0.7447	0.0000	80	Al–Al	0.274
47	Al	0.0908	0.6144	0.5000	51	Al–Al	0.281
51	Al	0.1855	0.7225	0.5000	47	Al–Al	0.281
52	Al	0.1738	0.4798	0.5000	70	Al–Al	0.281
61	Al	0.8145	0.5275	0.5000	65	Al–Al	0.281
62	Al	0.8262	0.7702	0.5000	86	Al–Al	0.281
65	Al	0.9092	0.6356	0.5000	61	Al–Al	0.281
71	Al	0.3145	0.5275	0.0000	77	Al–Al	0.281
72	Al	0.3262	0.7702	0.0000	54	Al–Al	0.281
77	Al	0.4092	0.6356	0.0000	71	Al–Al	0.281
79	Al	0.5908	0.6144	0.0000	83	Al–Al	0.281
83	Al	0.6855	0.7225	0.0000	79	Al–Al	0.281
84	Al	0.6738	0.4798	0.0000	60	Al–Al	0.281
53	Al	0.4526	0.5708	0.5000	59	Al–Al	0.282
55	Al	0.3661	0.7016	0.5000	54	Al–Al	0.282
57	Al	0.6339	0.5484	0.5000	60	Al–Al	0.282
59	Al	0.5474	0.6792	0.5000	53	Al–Al	0.282
67	Al	0.1339	0.5484	0.0000	70	Al–Al	0.282
69	Al	0.0474	0.6792	0.0000	85	Al–Al	0.282
85	Al	0.9526	0.5708	0.0000	69	Al–Al	0.282
87	Al	0.8661	0.7016	0.0000	86	Al–Al	0.282
49	Al	0.2712	0.5923	0.5000	55	Al–Al	0.284
63	Al	0.7288	0.6577	0.5000	57	Al–Al	0.284
73	Al	0.2288	0.6577	0.0000	67	Al–Al	0.284
81	Al	0.7712	0.5923	0.0000	87	Al–Al	0.284
54	Al	0.4585	0.8102	0.5000	24	Al–Si	0.262
60	Al	0.5415	0.4398	0.5000	28	Al–Si	0.262
70	Al	0.0415	0.4398	0.0000	26	Al–Si	0.262
86	Al	0.9585	0.8102	0.0000	22	Al–Si	0.262
50	Al	0.2799	0.8323	0.5000	36	Al–Si	0.263
64	Al	0.7201	0.4177	0.5000	32	Al–Si	0.263
74	Al	0.2201	0.4177	0.0000	30	Al–Si	0.263
82	Al	0.7799	0.8323	0.0000	34	Al–Si	0.263
48	Al	0.0981	0.8494	0.5000	22	Al–Si	0.265
66	Al	0.9019	0.4006	0.5000	26	Al–Si	0.265
78	Al	0.4019	0.4006	0.0000	28	Al–Si	0.265
80	Al	0.5981	0.8494	0.0000	24	Al–Si	0.265
56	Al	0.3545	0.4624	0.5000	44	Al–Si	0.276
58	Al	0.6455	0.7876	0.5000	40	Al–Si	0.276
68	Al	0.1455	0.7876	0.0000	38	Al–Si	0.276
88	Al	0.8545	0.4624	0.0000	42	Al–Si	0.276

Table A3

Atomic positions for interfacial supercell C<sub>4</sub>

Index	Symbol	Internal position			Nearest neighboring atom		
		x	y	z	Index	Bond type	Distance (nm)
1	Mg	0.0107	0.9948	0.0000	22	Mg–Si	0.271
2	Mg	0.9893	0.2552	0.0000	26	Mg–Si	0.271
3	Mg	0.5107	0.9948	0.5000	24	Mg–Si	0.271
4	Mg	0.4893	0.2552	0.5000	28	Mg–Si	0.271
13	Mg	0.4198	0.1589	0.0000	23	Mg–Si	0.278
15	Mg	0.9198	0.1589	0.5000	21	Mg–Si	0.278
17	Mg	0.5802	0.0911	0.0000	27	Mg–Si	0.278
19	Mg	0.0802	0.0911	0.5000	25	Mg–Si	0.278
5	Mg	0.3521	0.0137	0.0000	27	Mg–Si	0.281
7	Mg	0.8521	0.0137	0.5000	25	Mg–Si	0.281
9	Mg	0.6479	0.2363	0.0000	23	Mg–Si	0.281
11	Mg	0.1479	0.2363	0.5000	21	Mg–Si	0.281
6	Mg	0.3337	0.2720	0.0000	30	Mg–Si	0.284
8	Mg	0.8337	0.2720	0.5000	32	Mg–Si	0.284
10	Mg	0.6663	0.9780	0.0000	34	Mg–Si	0.284
12	Mg	0.1663	0.9780	0.5000	36	Mg–Si	0.284
14	Mg	0.4279	0.8962	0.0000	24	Mg–Si	0.286
16	Mg	0.9279	0.8962	0.5000	22	Mg–Si	0.286
18	Mg	0.5721	0.3538	0.0000	28	Mg–Si	0.286
20	Mg	0.0721	0.3538	0.5000	26	Mg–Si	0.286
21	Si	0.0524	0.1688	0.0000	37	Si–Si	0.237
23	Si	0.5524	0.1688	0.5000	39	Si–Si	0.237
25	Si	0.9476	0.0812	0.0000	41	Si–Si	0.237
27	Si	0.4476	0.0812	0.5000	43	Si–Si	0.237
37	Si	0.2053	0.1581	0.0000	21	Si–Si	0.237

Table A4  
Atomic positions for interfacial supercell B<sub>1</sub>

Index	Symbol	Internal position			Nearest neighboring atom		
		x	y	z	Index	Bond type	Distance (nm)
2	Mg	0.0000	0.0000	0.2779	22	Mg–Si	0.266
3	Mg	0.5000	0.0000	0.0971	23	Mg–Si	0.266
1	Mg	0.0000	0.0000	0.9818	21	Mg–Si	0.274
4	Mg	0.5000	0.0000	0.3932	24	Mg–Si	0.274
6	Mg	0.3494	0.0682	0.2402	28	Mg–Si	0.275
7	Mg	0.8494	0.0682	0.1348	25	Mg–Si	0.275
10	Mg	0.6506	0.9318	0.2402	24	Mg–Si	0.275
11	Mg	0.1506	0.9318	0.1348	21	Mg–Si	0.275
14	Mg	0.4295	0.6526	0.2437	24	Mg–Si	0.277
15	Mg	0.9295	0.6526	0.1313	21	Mg–Si	0.277
18	Mg	0.5705	0.3474	0.2437	28	Mg–Si	0.277
19	Mg	0.0705	0.3474	0.1313	25	Mg–Si	0.277
5	Mg	0.3288	0.0593	0.0025	27	Mg–Si	0.279
8	Mg	0.8288	0.0593	0.3725	26	Mg–Si	0.279
9	Mg	0.6712	0.9407	0.0025	23	Mg–Si	0.279
12	Mg	0.1712	0.9407	0.3725	22	Mg–Si	0.279
22	Si	0.0553	0.6736	0.2586	26	Si–Si	0.236
23	Si	0.5553	0.6736	0.1164	27	Si–Si	0.236
26	Si	0.9447	0.3264	0.2586	22	Si–Si	0.236
27	Si	0.4447	0.3264	0.1164	23	Si–Si	0.236
21	Si	0.0592	0.6704	0.0125	25	Si–Si	0.237
24	Si	0.5592	0.6704	0.3625	28	Si–Si	0.237
25	Si	0.9408	0.3296	0.0125	21	Si–Si	0.237
28	Si	0.4408	0.3296	0.3625	24	Si–Si	0.237
37	Si	0.2076	0.6221	0.0071	21	Si–Si	0.237
40	Si	0.7076	0.6221	0.3679	24	Si–Si	0.237
41	Si	0.7924	0.3779	0.0071	25	Si–Si	0.237
44	Si	0.2924	0.3779	0.3679	28	Si–Si	0.237
38	Si	0.2051	0.6347	0.2405	22	Si–Si	0.238
39	Si	0.7051	0.6347	0.1345	23	Si–Si	0.238
42	Si	0.7949	0.3653	0.2405	26	Si–Si	0.238
43	Si	0.2949	0.3653	0.1345	27	Si–Si	0.238
29	Si	0.1886	0.2537	0.0202	37	Si–Si	0.243
30	Si	0.1917	0.2562	0.2516	44	Si–Si	0.243
31	Si	0.6917	0.2562	0.1234	41	Si–Si	0.243
32	Si	0.6886	0.2537	0.3548	40	Si–Si	0.243
33	Si	0.8114	0.7463	0.0202	41	Si–Si	0.243
34	Si	0.8083	0.7438	0.2516	40	Si–Si	0.243
35	Si	0.3083	0.7438	0.1234	37	Si–Si	0.243
36	Si	0.3114	0.7463	0.3548	44	Si–Si	0.243
52	Al	0.2091	0.9098	0.7586	69	Al–Al	0.270
54	Al	0.4580	0.2878	0.6905	71	Al–Al	0.270
60	Al	0.5420	0.7122	0.6905	83	Al–Al	0.270
62	Al	0.7909	0.0902	0.7586	85	Al–Al	0.270
69	Al	0.0420	0.7122	0.6845	52	Al–Al	0.270
71	Al	0.2909	0.0902	0.6164	54	Al–Al	0.270
83	Al	0.7091	0.9098	0.6164	60	Al–Al	0.270
85	Al	0.9580	0.2878	0.6845	62	Al–Al	0.270
46	Al	0.0000	0.0000	0.7917	70	Al–Al	0.271
48	Al	0.1198	0.4364	0.7858	70	Al–Al	0.271
66	Al	0.8802	0.5636	0.7858	86	Al–Al	0.271
75	Al	0.5000	0.0000	0.5833	59	Al–Al	0.271
77	Al	0.3802	0.5636	0.5892	53	Al–Al	0.271
79	Al	0.6198	0.4364	0.5892	59	Al–Al	0.271
47	Al	0.0637	0.3930	0.5458	49	Al–Al	0.273
65	Al	0.9363	0.6070	0.5458	63	Al–Al	0.273
78	Al	0.4363	0.6070	0.8292	74	Al–Al	0.273
80	Al	0.5637	0.3930	0.8292	82	Al–Al	0.273
50	Al	0.2851	0.3779	0.7372	78	Al–Al	0.274
64	Al	0.7149	0.6221	0.7372	80	Al–Al	0.274
73	Al	0.2149	0.6221	0.6378	47	Al–Al	0.274
81	Al	0.7851	0.3779	0.6378	65	Al–Al	0.274

Table A4 (continued)

Index	Symbol	Internal position			Nearest neighboring atom		
		x	y	z	Index	Bond type	Distance (nm)
51	Al	0.1271	0.8372	0.5356	65	Al–Al	0.275
61	Al	0.8729	0.1628	0.5356	47	Al–Al	0.275
72	Al	0.3729	0.1628	0.8394	80	Al–Al	0.275
84	Al	0.6271	0.8372	0.8394	78	Al–Al	0.275
45	Al	0.0000	0.0000	0.4643	61	Al–Al	0.280
56	Al	0.3826	0.8551	0.7207	78	Al–Al	0.280
58	Al	0.6174	0.1449	0.7207	80	Al–Al	0.280
67	Al	0.1174	0.1449	0.6543	47	Al–Al	0.280
76	Al	0.5000	0.0000	0.9107	72	Al–Al	0.280
87	Al	0.8826	0.8551	0.6543	65	Al–Al	0.280
53	Al	0.4362	0.2798	0.5107	28	Al–Si	0.252
59	Al	0.5638	0.7202	0.5107	24	Al–Si	0.252
70	Al	0.0638	0.7202	0.8643	21	Al–Si	0.252
86	Al	0.9362	0.2798	0.8643	25	Al–Si	0.252
55	Al	0.3145	0.8341	0.5011	36	Al–Si	0.253
57	Al	0.6855	0.1659	0.5011	32	Al–Si	0.253
68	Al	0.1855	0.1659	0.8739	29	Al–Si	0.253
88	Al	0.8145	0.8341	0.8739	33	Al–Si	0.253
49	Al	0.2162	0.2849	0.5063	44	Al–Si	0.257
63	Al	0.7838	0.7151	0.5063	40	Al–Si	0.257
74	Al	0.2838	0.7151	0.8687	37	Al–Si	0.257
82	Al	0.7162	0.2849	0.8687	41	Al–Si	0.257
13	Mg	0.4022	0.5782	0.9950	78	Mg–Al	0.283
16	Mg	0.9022	0.5782	0.3800	65	Mg–Al	0.283
17	Mg	0.5978	0.4218	0.9950	80	Mg–Al	0.283
20	Mg	0.0978	0.4218	0.3800	47	Mg–Al	0.283

Table A5  
Atomic positions for interfacial supercell B<sub>2</sub>

Index	Symbol	Internal position			Nearest neighboring atom		
		x	y	z	Index	Bond type	Distance (nm)
2	Mg	0.0000	0.0000	0.2362	26	Mg–Si	0.260
3	Mg	0.5000	0.0000	0.1389	27	Mg–Si	0.260
1	Mg	0.0000	0.0000	0.0123	21	Mg–Si	0.269
4	Mg	0.5000	0.0000	0.3627	28	Mg–Si	0.269
5	Mg	0.3460	0.0799	0.0047	27	Mg–Si	0.275
8	Mg	0.8460	0.0798	0.3703	26	Mg–Si	0.275
9	Mg	0.6540	0.9201	0.0047	23	Mg–Si	0.275
12	Mg	0.1540	0.9202	0.3703	22	Mg–Si	0.275
6	Mg	0.3426	0.0801	0.2539	27	Mg–Si	0.277
7	Mg	0.8426	0.0800	0.1210	26	Mg–Si	0.277
10	Mg	0.6574	0.9199	0.2539	23	Mg–Si	0.277
11	Mg	0.1574	0.9200	0.1210	22	Mg–Si	0.277
14	Mg	0.4137	0.6074	0.2582	36	Mg–Si	0.285
15	Mg	0.9137	0.6074	0.1169	33	Mg–Si	0.285
16	Mg	0.9216	0.6159	0.3735	22	Mg–Si	0.285
18	Mg	0.5863	0.3926	0.2582	32	Mg–Si	0.285
19	Mg	0.0863	0.3926	0.1169	29	Mg–Si	0.285
20	Mg	0.0784	0.3841	0.3735	26	Mg–Si	0.285
13	Mg	0.4217	0.6160	0.0014	23	Mg–Si	0.286
17	Mg	0.5783	0.3840	0.0014	27	Mg–Si	0.286
22	Si	0.0568	0.6693	0.2458	26	Si–Si	0.236
23	Si	0.5568	0.6693	0.1292	27	Si–Si	0.236
26	Si	0.9432	0.3307	0.2458	22	Si–Si	0.236
27	Si	0.4432	0.3307	0.1292	23	Si–Si	0.236
38	Si	0.2122	0.6378	0.2508	22	Si–Si	0.240
39	Si	0.7122	0.6378	0.1241	23	Si–Si	0.240
42	Si	0.7878	0.3622	0.2508	26	Si–Si	0.240
43	Si	0.2878	0.3622	0.1241	27	Si–Si	0.240

Table A5 (continued)

Index	Symbol	Internal position			Nearest neighboring atom		
		x	y	z	Index	Bond type	Distance (nm)
21	Si	0.0623	0.6675	0.9896	25	Si–Si	0.242
24	Si	0.5623	0.6675	0.3854	28	Si–Si	0.242
25	Si	0.9377	0.3325	0.9896	21	Si–Si	0.242
28	Si	0.4377	0.3325	0.3854	24	Si–Si	0.242
30	Si	0.1915	0.2549	0.2501	38	Si–Si	0.247
31	Si	0.6915	0.2549	0.1249	39	Si–Si	0.247
34	Si	0.8085	0.7451	0.2501	42	Si–Si	0.247
35	Si	0.3085	0.7451	0.1249	43	Si–Si	0.247
37	Si	0.2238	0.6387	0.9851	21	Si–Si	0.248
40	Si	0.7238	0.6385	0.3901	24	Si–Si	0.248
41	Si	0.7762	0.3613	0.9851	25	Si–Si	0.248
44	Si	0.2762	0.3615	0.3901	28	Si–Si	0.248
29	Si	0.1910	0.2442	0.9993	43	Si–Si	0.249
32	Si	0.6910	0.2441	0.3757	42	Si–Si	0.249
33	Si	0.8090	0.7558	0.9993	39	Si–Si	0.249
36	Si	0.3090	0.7559	0.3757	38	Si–Si	0.249
46	Al	0.0000	0.0000	0.8435	88	Al–Al	0.270
55	Al	0.3515	0.8158	0.6291	75	Al–Al	0.270
57	Al	0.6485	0.1842	0.6291	75	Al–Al	0.270
68	Al	0.1485	0.1842	0.7459	46	Al–Al	0.270
75	Al	0.5000	0.0000	0.5315	57	Al–Al	0.270
88	Al	0.8515	0.8158	0.7459	46	Al–Al	0.270
53	Al	0.4462	0.2838	0.6235	75	Al–Al	0.273
59	Al	0.5538	0.7162	0.6235	75	Al–Al	0.273
70	Al	0.0538	0.7162	0.7515	46	Al–Al	0.273
86	Al	0.9462	0.2838	0.7515	46	Al–Al	0.273
49	Al	0.2734	0.3664	0.6211	67	Al–Al	0.277
54	Al	0.4556	0.2762	0.8618	72	Al–Al	0.277
56	Al	0.3655	0.8257	0.8664	74	Al–Al	0.277
58	Al	0.6345	0.1743	0.8664	82	Al–Al	0.277
60	Al	0.5444	0.7238	0.8618	84	Al–Al	0.277
63	Al	0.7266	0.6336	0.6211	87	Al–Al	0.277
67	Al	0.1345	0.1743	0.5086	49	Al–Al	0.277
72	Al	0.3172	0.0876	0.7484	54	Al–Al	0.277
74	Al	0.2266	0.6336	0.7539	56	Al–Al	0.277
82	Al	0.7734	0.3664	0.7539	58	Al–Al	0.277
84	Al	0.6828	0.9124	0.7484	60	Al–Al	0.277
87	Al	0.8655	0.8257	0.5086	63	Al–Al	0.277
51	Al	0.1827	0.9123	0.6266	69	Al–Al	0.278
61	Al	0.8173	0.0877	0.6266	85	Al–Al	0.278
69	Al	0.0444	0.7238	0.5131	51	Al–Al	0.278
85	Al	0.9556	0.2762	0.5131	61	Al–Al	0.278
47	Al	0.0901	0.4476	0.6329	85	Al–Al	0.279
65	Al	0.9099	0.5524	0.6329	69	Al–Al	0.279
78	Al	0.4099	0.5524	0.7421	60	Al–Al	0.279
80	Al	0.5901	0.4476	0.7421	54	Al–Al	0.279
45	Al	0.0000	0.0000	0.6352	88	Al–Al	0.283
76	Al	0.5000	0.0000	0.7398	57	Al–Al	0.283
50	Al	0.2830	0.3719	0.8667	29	Al–Si	0.257
64	Al	0.7170	0.6281	0.8667	33	Al–Si	0.257
73	Al	0.2170	0.6282	0.5083	36	Al–Si	0.257
81	Al	0.7830	0.3718	0.5083	32	Al–Si	0.257
48	Al	0.0897	0.4228	0.8691	21	Al–Si	0.267
66	Al	0.9103	0.5772	0.8691	25	Al–Si	0.267
77	Al	0.4103	0.5772	0.5059	28	Al–Si	0.267
79	Al	0.5897	0.4228	0.5059	24	Al–Si	0.267
52	Al	0.1803	0.9156	0.8781	21	Al–Si	0.272
62	Al	0.8197	0.0844	0.8781	25	Al–Si	0.272
71	Al	0.3197	0.0843	0.4970	28	Al–Si	0.272
83	Al	0.6803	0.9157	0.4970	24	Al–Si	0.272

## References

- [1] Andersen SJ, Marioara CD, Froseth A, Vissers R, Zandbergen HW. Mater Sci Eng A-Struct Mater Prop Microstruct Process 2005;390:127.
- [2] Marioara CD, Andersen SJ, Zandbergen HW, Holmestad R. Metall Mater Trans A-Phys Metall Mater Sci 2005;36A:691.
- [3] Matsuda K, Ikeno S, In: Primm 5: The fifth pacific rim international conference on advanced materials and processing, Pts 1-5 Zurich-Uetikon, Trans Tech Publications Ltd, 2005, p. 361.
- [4] Tsao CS, Jeng US, Chen CY, Kuo TY. Scr Mater 2005;53:1241.
- [5] Chen JH, Costan E, van Huis MA, Xu Q, Zandbergen HW. Science 2006;312:416.
- [6] Marioara CD, Nordmark H, Andersen SJ, Holmestad R. J Mater Sci 2006;41:471.
- [7] Matsuda K, Ishida Y, Mullerova I, Frank L, Ikeno S. J Mater Sci 2006;41:2605.
- [8] Tsao CS, Chen CY, Jeng US, Kuo TY. Acta Mater 2006;54:4621.
- [9] van Huis MA, Chen JH, Zandbergen HW, Sluiter MHF. Acta Mater 2006;54:2945.
- [10] Edwards GA, Stiller K, Dunlop GL, Couper MJ. Acta Mater 1998;46:3893.
- [11] Andersen SJ, Zandbergen HW, Jansen J, Traeholt C, Tundal U, Reiso O. Acta Mater 1998;46:3283.
- [12] Marioara CD, Andersen SJ, Jansen J, Zandbergen HW. Acta Mater 2001;49:321.
- [13] Andersen SJ, Marioara CD, Froseth A, Vissers R, Zandbergen HW. Electron microscopy and analysis 2003. Bristol: IOP Publishing Ltd.; 2004. p. 225.
- [14] Matsuda K, Kawabata T, Uetani Y, Sato T, Ikeno S. J Mater Sci 2002;37:3369.
- [15] Chen LQ, Shen J. Comput Phys Commun 1998;108:147.
- [16] Chen LQ. Ann Rev Mater Res 2002;32:113.
- [17] Zandbergen HW, Andersen SJ, Jansen J. Science 1997;277:1221.
- [18] Amini M, Laird BB. Phys Rev Lett 2006;97:216102.
- [19] Ouyang G, Liang LH, Wang CX, Yang GW. Appl Phys Lett 2006;88:091914.
- [20] Marquis EA, Seidman DN, Asta M, Woodward C, Ozolins V. Phys Rev Lett 2003;91:036101.
- [21] Vaithyanathan V, Wolverton C, Chen LQ. Phys Rev Lett 2002;88:125503.
- [22] Sluiter M, Kawazoe Y. Phys Rev B 1996;54:10381.
- [23] Sluiter M, Asta M, Kawazoe Y. Sci Rep Res Inst Tohoku Univ Ser A-Phys Chem Metall 1996;41:97.
- [24] Ravi C, Wolverton C. Acta Mater 2004;52:4213.
- [25] Vanderbilt D, Kingsmith RD. Phys Rev B 1993;48:4442.
- [26] Meyer B, Vanderbilt D. Phys Rev B 2001;63:205426.
- [27] Fennis MW. Phys Status Solidi A-Appl Res 1998;166:397.
- [28] Fennis MW, Lozovoi AY, Alavi A. Ann Rev Mater Res 2005;35:167.
- [29] Kresse G, Demuth T, Mittendorfer F. VAMP/VASP, <<http://cms.mpi.univie.ac.at/vasp/>>, 2003.
- [30] Kresse G, Furthmuller J. Comput Mater Sci 1996;6:15.
- [31] Kresse G, Furthmuller J. Phys Rev B 1996;54:11169.
- [32] Vanderbilt D. Phys Rev B 1990;41:7892.
- [33] Perdew JP, Wang Y. Phys Rev B 1992;45:13244.
- [34] Ozolins V, Wolverton C, Zunger A. Phys Rev B 1998;57:4816.
- [35] Vaithyanathan V, Wolverton C, Chen LQ. Acta Mater 2004;52:2973.
- [36] Winter MJ. WebElements Periodic table (professional edition), <http://www.webelements.com/>.
- [37] Wolverton C, Ozolins V. Phys Rev B 2006;73:064101.